

**NASA TECHNICAL MEMORANDUM 104210**

**An Evaluation of Mixed-Mode  
Delamination Failure Criteria**

**J. R. Reeder**

**FEBRUARY 1992**



**National Aeronautics and  
Space Administration**

**Langley Research Center  
Hampton, Virginia 23665-5225**

## **ABSTRACT**

Many different failure criteria have been suggested for mixed-mode delamination toughness, but few sets of mixed-mode data exist that are consistent over the full mode I opening to mode II shear load range. The mixed-mode bending (MMB) test was used to measure the delamination toughness of a brittle epoxy composite, a state-of-the-art toughened epoxy composite, and a tough thermoplastic composite over the full mixed-mode range. To gain insight into the different failure responses of the different materials, the delamination fracture surfaces were also examined. An evaluation of several failure criteria which have been reported in the literature was performed, and the range of responses modeled by each criterion was analyzed. A new bilinear failure criterion was developed based on a change in the failure mechanism observed from the delamination surfaces. The different criteria were compared to the failure response of the three materials tested. The responses of the two epoxies were best modeled with the new bilinear failure criterion. The failure response of the tough thermoplastic composite could be modeled well with the bilinear criterion but could also be modeled with the more simple linear failure criterion. Since the materials differed in their mixed-mode failure response, mixed-mode delamination testing will be needed to characterize a composite material. This paper provides a critical evaluation of the mixed-mode failure criteria and should provide general guidance for selecting an appropriate criterion for other materials.

## INTRODUCTION

Delamination is a primary failure mode of laminated composite materials. Delamination toughness under mode I opening load and mode II shear load can be measured with the double cantilever beam (DCB) test and the end notch flexure (ENF) test, respectively. In structures however, delaminations are not just loaded in pure mode I or pure mode II but grow under a mixture of mode I and mode II loading. Several types of tests have been used to measure mixed-mode delamination fracture toughness. In the past, several different kinds of test specimens were needed to measure delamination fracture toughness over the full range of mode I and mode II combinations<sup>1</sup>. Unfortunately it was unclear what effect the different test configurations had on the measured failure response. Recently however, the mixed-mode bending (MMB) test<sup>2</sup>, which simply combines the DCB and ENF loadings, was developed to measure mixed-mode delamination toughness and then redesigned<sup>3</sup> to avoid geometric nonlinearities encountered when testing tough composites. The MMB test allows almost any combination of mode I and mode II loading to be tested with the same test specimen configuration. Therefore, inconsistencies present in previous mixed-mode toughness data sets can be avoided.

Many different mixed-mode failure criteria have been suggested for predicting delamination growth, but these criteria were often based on inconsistent sets of toughness data. It is important that accurate mixed-mode failure criteria be developed so that the extension of delaminations in structures can be predicted. Once delamination can be predicted accurately, fewer component and full scale tests will be required to ensure the safety of composite structures. The purpose of this paper is to evaluate mixed-mode failure criteria by comparing them to consistent sets of mixed-mode toughness data obtained using the MMB test.

The redesigned mixed-mode bending (MMB) test was used to measure the delamination toughness of a brittle epoxy composite, a state-of-the-art toughened epoxy composite, and a tough thermoplastic composite over the full mixed-mode range. The fracture surfaces of the composites were examined to gain insight into the failure responses of the different materials. Next, an evaluation of delamination failure criteria which have been reported in the literature was performed, and the range of material responses modeled by each criterion was evaluated. In addition, a new bilinear failure criterion was introduced. The failure response of the three materials were compared to the different mixed-mode failure criteria, and the best criterion for each material was selected.

## **TOUGHNESS TESTING**

The redesigned MMB test apparatus was used to measure the mixed-mode delamination toughness of three different composite materials. This test is capable of testing over virtually the entire mixed-mode range with consistent test conditions. Consistent sets of data with which to compare proposed failure criteria therefore were obtained.

The materials used in this study were chosen to represent a wide range of toughness properties. AS4/3501-6 is a commonly used brittle epoxy composite. IM7/977-2 is a state-of-the-art toughened epoxy composite. It consists of a high strength IM7 fiber and an epoxy matrix which has been toughened with a thermoplastic additive. The AS4/PEEK (polyether-ether-ketone) is a tough graphite/thermoplastic composite and therefore radically different from the thermoset epoxies. The elastic properties of these three materials are listed in Table 1. These properties were used in the calculation of fracture toughness. Because the toughness calculation is very sensitive to the longitudinal modulus  $E_{11}$ , it was measured using a

3-point bend test with a 3 inch span length.  $E_{11}$  was measured in bending because for composite materials a flexurally measured modulus has been shown to differ significantly from an axially measured modulus,<sup>4</sup> and the MMB test is a bending type of test. The toughness calculation is not as sensitive to the transverse modulus  $E_{22}$  and shear modulus  $G_{13}$ . Therefore, these properties were obtained from the literature<sup>3,5,6</sup>.

The materials were made into 24 ply unidirectional panels. The panels were cut into test specimen which were 6 in. long, 1 in. wide,  $b$ , and nominally 0.12 in. thick,  $2h$ . Each specimen contained a 0.5 mil thick insert at the midplane of the specimen to act as a delamination starter. A Teflon insert was used in the epoxy specimens while a Kapton insert was used in the PEEK specimens. Hinges were bonded to the specimens as shown in Figure 1, so that the starter provided a 1 inch initial delamination length  $a$ .

The redesigned MMB test apparatus shown in Figure 1 uses a lever to apply mode I and mode II loadings to a split beam specimen. The load on the top hinge tends to pull the delamination open resulting in mode I loading similar to that of the DCB test. The load at the fulcrum bends the specimen creating a mode II loading similar to the ENF test. The ratio of the mode I to mode II loading is controlled by the lever load position,  $c$ . The value of  $c$  therefore determines the mixed-mode ratio  $G_I/G_{II}$ . The redesigned apparatus uses a saddle mechanism to hold the loading rollers just above the specimen mid-plane and on either side of the test specimen. This configuration has been shown to drastically reduce geometric nonlinearity errors which can develop when testing tough materials<sup>3</sup>. The half span length  $L$  of the MMB apparatus was 2 inches.

Each material was tested in at least three mixed-mode ratios ( $G_I/G_{II}$ ) and at the two pure-mode cases. The three mixed-mode ratios tested were the 4/1, 1/1, and 1/4 cases which corresponded to  $c$  values of 3.83 in. , 1.66 in., and 1.09 in., respectively. The AS4/3501-6 material was also tested at a 1/20 ratio with a  $c$  value 0.85 in. while the IM7/977-2 material was tested at the 1/2 ratio with a  $c$  value of 1.30 in. The pure

mode I toughness was tested using a standard DCB configuration. The pure mode II toughness was tested using the MMB apparatus with a  $c$  value of 0. This is equivalent to an ENF configuration. All the tests are consistent since the mixed-mode test is simply a combination of the pure-mode tests. Five tests at each test configuration were performed on the epoxies while only 3 tests were performed for the PEEK material.

The specimens were loaded in displacement control at a rate of 0.02 in/min at the lever loading point. The load-displacement response was recorded, and the critical load used in  $G_c$  calculations was taken as the load where the load-displacement curve deviated from linearity. The tests on the epoxy specimen measured the toughness required for delamination to initiate from the insert. The PEEK specimen which were tested in a previous study<sup>3</sup> were first precracked under a 4/1 mixed-mode loading to a delamination length  $a$  of 1.25 in. and then tested. Although Murri et. al.<sup>7</sup> showed that delamination toughness measured from a precrack could be significantly different from values measured from an insert, a study involving a 4/1 type precrack showed good agreement with insert initiation values.<sup>8</sup> The critical applied load  $P_c$  for all tests were taken as the load where the load displacement curve deviates from linear. The PEEK toughnesses presented here is slightly lower than that given in Reference 3 because that data was calculated with  $P_c$  equal to the maximum applied load. The edge of the specimen was coated with a white water soluble typewriter correction fluid so that the delamination could be observed more easily with a 7x magnifying scope. The delamination extension was observed at approximately the same time as the nonlinearity in the loading curve. The delamination length,  $a$ , was determined by breaking the test specimen open after the test and measuring the length of the initial delamination. For the epoxy specimen this was the length of the insert while for the PEEK specimen,  $a$  was the length to the marking on the fracture surface left by the precrack.

The mixed-mode fracture toughness,  $G_{Ic}^m$  and  $G_{IIc}^m$ , of the IM7/977-2 and AS4/PEEK specimen were calculated using the following equations:

$$G_{Ic}^m = \frac{(36c^2 - 24cL + 4L^2)P_c^2}{64L^2bE_{11}I} \left[ a^2 + \frac{2a}{\lambda} + \frac{1}{\lambda^2} + \frac{h^2E_{11}}{10G_{13}} \right]$$

$$G_{IIc}^m = \frac{(3c^2 + 6cL + 3L^2)P_c^2}{64L^2bE_{11}I} \left[ a^2 + \frac{.2h^2E_{11}}{G_{13}} \right] \quad (1)$$

$$\text{where } \lambda = \frac{1}{h} \sqrt[4]{\frac{6E_{22}}{E_{11}}} \quad \text{and} \quad I = \frac{bh^3}{12}$$

These equations are based on beam theory and include corrections to account for shear deformation and deformation due to the rotation of the specimen cross section at the delamination tip<sup>2</sup>.

The fracture toughness calculation of the AS4/3501-6 was more complicated. The complication arose because the toughness of this material is small compared to the other two materials resulting in smaller critical applied loads  $P_c$ . The critical loads in some cases were of the same magnitude as the lever weight  $P_g$  ( $P_g=1.85$  lb,  $P_c=10$  lb), and therefore, the lever weight could not be ignored. A derivation of how the lever weight was included is presented in Appendix A, and the resulting equations for mixed-mode fracture toughness are:

$$G_{Ic}^m = \left[ \begin{array}{l} (36c^2 - 24cL + 4L^2)P_c^2 + \\ (72cc_g - 24cL - 24c_gL + 8L^2)P_cP_g + \\ (36c_g^2 - 24c_gL + 4L^2)P_g^2 \end{array} \right] \frac{\left[ a^2 + \frac{2a}{\lambda} + \frac{1}{\lambda^2} + \frac{h^2E_{11}}{10G_{13}} \right]}{64L^2bE_{11}I}$$

$$G_{IIc}^m = \left[ \begin{array}{l} (3c^2 + 6cL + 3L^2)P_c^2 + \\ (6cc_g + 6cL + 6c_gL + 6L^2)P_cP_g + \\ (3c_g^2 + 6c_gL + 3L^2)P_c^2 \end{array} \right] \frac{\left[ a^2 + \frac{.2h^2E_{11}}{G_{13}} \right]}{64L^2bE_{11}I} \quad (2)$$

The equations in the appendix are written in terms of an applied load  $P_a$  and strain energy release rates,  $G_I$  and  $G_{II}$ , while Eqs. 2 are written in terms of a critical load  $P_c$  and the fracture toughnesses,  $G_{Ic}^m$  and  $G_{IIc}^m$ . Appendix A also includes criteria for deciding when the lever weight corrections are needed.

The pure mode I toughness was calculated using Equation 3 for all materials.

$$G_{Ic} = \frac{P_c^2}{bE_{11}I} \left[ a^2 + \frac{2a}{\lambda} + \frac{1}{\lambda^2} + \frac{h^2 E_{11}}{10G_{13}} \right] \quad (3)$$

This equation was used in developing the mixed-mode equations and is consistent with the mixed-mode equations. The pure mode II toughness  $G_{IIc}$  can be calculated from the equations for  $G_{IIc}^m$  in Equations 1 or 2 where  $c$  is set to 0. Notice that the  $G_{IIc}^m$  equations give erroneous results at this  $c$  value because for  $c \lesssim 0.67$ , the delamination surfaces do not separate. The contact forces across the delamination surfaces which are not modeled by Equation 1 and 2 cause the true  $G_{IIc}^m$  to be 0 but do not effect the  $G_{IIc}^m$  values.

The delamination fracture surfaces were examined using a scanning electron microscope (SEM). SEM photomicrographs were taken just beyond the delamination insert for the epoxy composites and just beyond the precrack marking for the PEEK composite. Therefore, the fracture surfaces show the first increment of delamination growth which correspond to the measured fracture toughnesses.

## TOUGHNESS TEST RESULTS

The mixed-mode failure responses of the three composite materials are presented by plotting the mode I component of fracture toughness,  $G_{Ic}^m$  vs. the mode II component,  $G_{IIc}^m$ . These mixed-mode diagrams are plotted in Figure 2. The failure response of the two epoxy composites are quite similar in shape, but the AS4/3501-6 material is more brittle than the IM7/977-2. For both epoxies, the  $G_{Ic}^m$  values appear

to increase as the  $G_{IIc}^m$  is introduced and then slowly decrease to zero as  $G_{IIc}^m$  approaches  $G_{IIc}$ . The rising  $G_{Ic}^m$  with  $G_{IIc}^m$  may be somewhat surprising, but this phenomenon can also be seen in data presented in References <sup>9</sup> and <sup>10</sup>. The overall shape of the failure response is convex and very similar in shape to the mixed-mode diagram for a brittle-epoxy composite system studied in Reference 1. The AS4/PEEK material is even tougher than the IM7/977-2 material at all mixed-mode ratios except near pure mode II and the shape of the failure response is quite different.  $G_{Ic}^m$  decreases almost linearly with  $G_{IIc}^m$  which produces a mixed-mode diagram very similar to those presented in Reference 1 for different tough composite systems. Since the shape of the failure responses of the different materials are so different, it is clear that no single criterion based on just  $G_{Ic}$  and  $G_{IIc}$  will model all delamination failure. One criteria might be able to model the different materials if arbitrary parameters can be changed so that the criterion can be fit to the data. If this does not work then different criteria would have to be used for different materials.

SEM photomicrographs show that the fracture surfaces of the different materials change dramatically with mixed-mode ratio. As discussed earlier, these photomicrographs were taken just after delamination initiation. Figure 3 shows the delamination surfaces at different mixed-mode ratios for the AS4/3501-6 composite. The photomicrographs were taken at a magnification of 1000x. At pure mode I the fracture surface is very flat indicating a brittle cleavage fracture which would explain the low mode I fracture toughness. As mode II is added, the fracture surfaces becomes rougher as seen in the 4/1 ratio case. Troughs have appeared where fibers have been pulled away from the matrix indicating interfacial failure. The side of the fracture surface which did not contain a large percentage of fibers is shown here because the texture of the fractured resin is easier to see in this view. The increase roughness could explain why the mode I component of fracture toughness rises as mode II is introduced. At the 1/1 ratio, hackles<sup>11</sup> have appeared, and there is little difference between the 1/1

fracture surface and the pure mode II. The similarity between the 1/1 and pure mode II fracture surfaces indicates a single failure mode through this region. The difference between these fracture surfaces and those at the pure mode I and 4/1 case may indicate a change in the failure mechanism around the 1/1 ratio.

Figure 4 shows the fracture surfaces of the IM7/977-2 composite at several mixed-mode ratios. As seen from the figure, the fracture surfaces of IM7/977-2 are very similar to that of AS4/3501-6. The mode I fracture is cleavage, fiber troughs appear at the 4/1 ratio, and hackling begins around the 1/1 ratio and continues through the pure mode II condition. The change in fracture surface between the 4/1 and 1/1 ratio is even more clear for this material than for the AS4/3501-6, and again may indicate a changing failure mechanism. The similarity in the fracture surfaces of these materials may explain the similarity between the shapes of the failure responses of these two materials which can be seen in Figure 2. No indication of the increased toughness of IM7/977-2 over AS4/3501-6 was noted by observing the fracture surfaces.

The fracture surfaces of the Peek composite shown in Figure 5 are noticeably different from that of the epoxies. All the PEEK fracture surfaces have cusps caused by the extensive yielding of the matrix. The larger strain to failure created by the yielding gives this material a larger fracture toughness than the epoxies tested. The ridges and valleys seen in the figure are due to the fibers which have been pulled out of the valleys. The ridges form because the larger volume of matrix material found between the fibers can deform more creating the ridges of cusps. The primary difference between the fracture surfaces at different mixed-mode ratios is the orientation of the cusps. The DCB fracture surface has cusps that are randomly pulled in different directions. In the 1/1 fracture surface the cusps tend to be drawn slightly toward the top of the micrograph due to the mode II action. Larger amounts of mode II draw the cusps more and more, and in the ENF fracture surfaces, all the cusps are

extensively drawn upward. No indication of hackling or of changing failure mechanism was observed on the AS4/PEEK fracture surfaces

## **REVIEW OF MIXED-MODE DELAMINATION CRITERIA**

Many attempts have been made at describing the mixed-mode delamination failure response of composite materials. Failure criterion have been based on stress or strain near the crack tip, crack opening displacement, stress intensity factor, or strain energy release rate. Strain energy release rate seems to be a good measure of a materials resistance to delamination extension and most of the failure criteria that have been suggested can be written in terms of a critical strain energy release rate or fracture toughness. Delamination fracture toughness testing under pure mode I loading and pure mode II loading is well established. Delaminations in structures are often subjected to mixed-mode loading so mixed-mode fracture toughness is also important. Since the mode I and mode II fracture toughness data is readily available, the mixed-mode failure criteria will be written in terms of the pure-mode toughnesses,  $G_{Ic}$  and  $G_{IIc}$ , when possible. Although the primary interest here is delamination, criteria suggested for both delamination and ply cracking will be presented. In both ply cracking and delamination, a crack is growing in the matrix in the direction of the fibers. Because the fiber-matrix geometry of both types of cracks are so similar, one would expect the failure responses to be similar as well.

The mixed-mode failure response of a material can be described by plotting the mode I component of fracture toughness,  $G_{Ic}^m$  vs. the mode II component,  $G_{IIc}^m$ . An accurate failure criterion will match the material response when plotted on this mixed-mode diagram. Since the the material response of different materials can be quite different, each failure criterion will be evaluated first by looking at the range of shapes each criterion can model. For comparison each criterion will be evaluated assuming

$G_{Ic} = 1$  and  $G_{IIc} = 3$ . Some criteria also involve the ratio of  $E_{11}/E_{22}$ . For comparison this ratio will be assumed to be 10. Later criteria will be fit to measured toughness data.

The simplest criteria assume that either the mode I component<sup>12</sup>, the mode II component<sup>13</sup>, or total fracture toughness<sup>14</sup> will stay constant as the mixed-mode ratio changes. These criteria are respectively:

$$G_{Ic}^m = G_{Ic} \quad (4)$$

$$G_{IIc}^m = G_{IIc} \quad (5)$$

$$G_{Ic}^m + G_{IIc}^m = G_{Tc} \quad ( = G_{Ic} = G_{IIc} ) \quad (6)$$

These criteria are plotted on the mixed-mode diagram ( $G_I$  vs.  $G_{II}$ ) in Figure 6. The first criterion assumes that only the mode I component of loading controls delamination growth which therefore assumes an infinite  $G_{IIc}$ . The second assumes that only the mode II component of loading is important and therefore an infinite  $G_{Ic}$ . A more reasonable criterion would be to combine the  $G_I$  and  $G_{II}$  criteria(Eqs. 4 & 5) by assuming that delamination growth would occur if either Equation 4 or 5 is met. This criterion then models the assumption that the mode I and mode II failure processes occur independently of each other. The third criterion assumes that a delamination will extend if the total strain energy  $G_{Tc}$  reaches some critical value. The fracture toughness is assumed not to be a function of mixed-mode ratio which means that  $G_{Ic}$  should equal  $G_{IIc}$ . Since  $G_{Ic}$  and  $G_{IIc}$  are known to be quite different for most materials, the  $G_{Tc}$  criterion(Eq. 6) was modified to account for materials with different mode I and mode II toughnesses as seen in the next criterion.

The fourth criterion simply normalizes each component of fracture toughness by its pure-mode value as given by<sup>14</sup>

$$\left(\frac{G_{Ic}^m}{G_{Ic}}\right) + \left(\frac{G_{IIc}^m}{G_{IIc}}\right) = 1 \quad (7)$$

The resulting curve on the mixed-mode fracture toughness diagram is a line connecting the pure mode I and pure mode II fracture toughnesses as shown on Figure 6. This linear criterion(Eq. 7) is perhaps the mixed-mode criterion most often referred to in literature<sup>1,10,15,16,17</sup>.

A fifth criterion is obtained by generalizing the linear criterion(Eq. 7) as a power law function<sup>12</sup> as follows:

$$\left(\frac{G_{Ic}^m}{G_{Ic}}\right)^\alpha + \left(\frac{G_{IIc}^m}{G_{IIc}}\right)^\beta = 1 \quad (8)$$

By choosing  $\alpha$  and  $\beta$ , a wide range of material responses can be modeled as shown in Figure 7. When  $\alpha=\beta>1$  the failure curve is convex while when  $\alpha=\beta<1$  the curve is concave. If  $\beta>\alpha$  then the curve is skewed so that the curve is more convex near the mode I axis. Besides  $\alpha=\beta=1$  which reproduces the linear criterion(Eq. 7) several  $(\alpha,\beta)$  combinations have been used such as (2,2)<sup>18</sup>, (0.5,1)<sup>14</sup>, (1,1.5)<sup>19</sup>, (1.4,1.8)<sup>20</sup>, (.64, .8)<sup>20</sup>. An optimum value of  $\alpha$  and  $\beta$  for a given material can be found by curve fitting through experimental data.

Another criterion was developed by assuming that the total fracture toughness would be a polynomial function<sup>21</sup> of the ratio of mode II to mode I as given by

$$G_{Ic}^m + G_{IIc}^m = G_{Ic} + \rho \left(\frac{G_{IIc}^m}{G_{Ic}^m}\right) + \tau \left(\frac{G_{IIc}^m}{G_{Ic}^m}\right)^2 \quad (9)$$

The polynomial criterion(Eq. 9) can model a wide variety of material responses by adjusting  $\rho$  and  $\tau$  as seen in Figure 8. This criterion can model both concave and convex failure curves. It is also the first criterion discussed which can allow the mode I to increase as mode II is introduced as seen when  $\rho=1.5$ . This material behavior is exhibited by the epoxy composite systems of the present investigation. However, this

criterion is unable to model low mode I to mode II ratios. Either the  $G_{Ic}^m$  gets very large or both  $G_{Ic}^m$  and  $G_{IIc}^m$  will go to zero as the mixed-mode ratio is decreased. Neither response is realistic, and therefore this criterion is an inappropriate choice as a general mixed-mode criterion.

Another criterion was developed by assuming the fracture toughness to be a linear function of the mode I stress intensity factor<sup>22</sup>  $K_{Ic}$ . This criterion has been written here in terms of  $G_{Ic}^m$  and  $G_{IIc}^m$  as

$$G_{Ic}^m + G_{IIc}^m = G_{IIc} - (G_{IIc} - G_{Ic}^m) \sqrt{G_{Ic}^m / G_{Ic}} \quad (10)$$

If  $G_{Ic} = G_{IIc}$  the  $K_{Ic}$  criterion (Eq. 10) reduces to the linear criterion (Eq. 7). If  $G_{Ic} \ll G_{IIc}$  then the  $K_{Ic}$  criterion (Eq. 10) reduces to the power law criterion (Eq. 8) where  $\alpha = .5$  and  $\beta = 1$ . This criteria is completely defined by the  $G_{Ic}$  and  $G_{IIc}$  values and produces a concave failure envelope as seen in Figure 9.

The next criterion was developed by modeling delamination growth through hackle formation<sup>23</sup>. The hackle criterion (Eq. 11) was based on a linear function of  $\sqrt{1 + (K_{II}/K_I)^2}$  which is a measure of the hackle angle. The criterion is written here in terms of the pure-mode fracture toughnesses, modulus values, and an arbitrary constant  $\chi$ .

$$G_{Ic}^m + G_{IIc}^m = (G_{Ic} - \chi) + \chi \sqrt{1 + \frac{G_{IIc}^m}{G_{Ic}^m} \sqrt{\frac{E_{11}}{E_{22}}}} \quad (11)$$

The hackle criterion (Eq. 11) is plotted on the mixed-mode diagram in Figure 10.  $\chi$  can be chosen to model a variety of material responses, including an increasing  $G_{Ic}^m$  with  $G_{IIc}^m$  as seen when  $\chi = 1$ . However, except for when  $\chi = 0$  which gives the  $G_{Ic}$  criterion (Eq. 6), the hackle criterion (Eq. 11) will always predict an infinite  $G_{IIc}$  so this criterion is also an inappropriate choice as a general mixed-mode criterion.

A second criterion was based on the hackle angle parameter  $\sqrt{1+(K_{II}/K_I)^2}$ , but this time it is related as an exponential instead of a linear function<sup>10</sup>. The exponential hackle criterion(Eq. 12) can also be written in terms of the pure-mode toughness values and only one arbitrary constant  $\gamma$  as follows:

$$G_{Ic}^m + G_{IIc}^m = (G_{Ic} - G_{IIc})e^{\gamma(1-N)} + G_{IIc} \quad N = \sqrt{1 + \frac{G_{IIc}^m}{G_{Ic}^m} \sqrt{\frac{E_{11}}{E_{22}}}} \quad (12)$$

This exponential hackle criterion(Eq. 12) has the advantage that it does model a finite  $G_{IIc}$  as seen in Figure 11. The  $\gamma$  constant can be chosen to model a great variety of material responses. The failure envelope can be concave or convex and it can model an increasing  $G_{Ic}^m$  with increasing  $G_{IIc}^m$ .

Another mixed-mode criterion was based on an exponential function of the mixed-mode stress intensity factor ratio<sup>24</sup>  $K_{Ic}/K_{IIc}$ . The criterion has been written here in terms of strain energy release rates and the arbitrary constant  $\eta$ .

$$G_{Ic}^m + G_{IIc}^m = (G_{IIc} - G_{Ic})e^{\eta\sqrt{G_{Ic}^m/G_{IIc}^m}} + G_{Ic} \quad (13)$$

The exponential  $K_{Ic}/K_{IIc}$  criterion(Eq. 13) is plotted on the mixed-mode diagram in Figure 12. This criterion can model the same types of responses modeled by the exponential hackle criterion(Eq. 12), but a strange jog in the failure curve near the mode I axis is introduced for  $\eta \leq 1$ .

Critical crack opening displacement (COD) was the basis of yet another criterion. A delamination is assumed to extend when the mode I or mode II critical crack opening displacement is reached. A Dugdale plasticity model was used to derive the following criterion<sup>25</sup>:

$$\begin{aligned}\frac{G_{IIc}^m}{G_{IIc}} &= \frac{1}{3} \sqrt{\frac{E_{22}}{E_{11}}} \left( \frac{G_{Ic}}{G_{Ic}^m} - \frac{G_{Ic}^m}{G_{Ic}} \right) \\ \frac{G_{Ic}^m}{G_{Ic}} &= 3 \sqrt{\frac{E_{11}}{E_{22}}} \left( \left( \frac{G_{IIc}}{G_{Ic}} \right)^2 \frac{G_{Ic}}{G_{IIc}^m} - \frac{G_{IIc}^m}{G_{Ic}} \right)\end{aligned}\quad (14)$$

The first equation assumes a critical mode I crack opening displacement while the second assumes a critical mode II displacement. The delamination is assumed to extend if either criterion is met. This criterion is plotted on the mixed-mode diagram in Figure 13. The COD criterion (Eq. 14) is plotted with  $E_{11}/E_{22}$  equal to both 10 and 1. The higher ratio corresponds to the ratio of global stiffnesses. Since this criterion is based on crack opening displacement, a localized phenomenon, a local stiffness ratio corresponding to a crack in an isotropic matrix material and therefore the lower ratio, may be more appropriate. With either stiffness ratio, the mode I criterion, which produces a concave failure response, is critical for most of the  $G_I/G_{II}$  values.

Another criterion was developed based on a mode I-mode II interaction parameter  $\kappa$ <sup>26</sup>.

$$\left( \frac{G_{Ic}^m}{G_{Ic}} - 1 \right) \left( \frac{G_{IIc}^m}{G_{IIc}} - 1 \right) - \kappa \left( \frac{G_{Ic}^m}{G_{Ic}} \right) \left( \frac{G_{IIc}^m}{G_{IIc}} \right) = 0 \quad (15)$$

The arbitrary interaction parameter  $\kappa$  is a measure of how much effect the mode I and mode II loadings have on each other. As shown in Figure 14, this criterion can describe both concave and convex material responses. If  $\kappa=0$  then the fracture modes are independent and the criterion is the same as combining the  $G_{Ic}$  and  $G_{IIc}$  criteria (Eqs. 4 & 5), and if  $\kappa=2$  the criterion is the same as the linear criterion (Eq. 7). The material responses modeled by this criterion seem to be almost identical to those modeled by the power law criterion (Eq. 8) when the arbitrary constants of the power law are equal. Values of  $\kappa$  from 0.26 to 3.12<sup>27</sup> have been suggested for different materials.

The interaction criterion was made more versatile by allowing the interaction parameter to be a linear function of  $G_{Ic}^m / (G_{Ic}^m + G_{IIc}^m)$  as given by<sup>28</sup>

$$\left(\frac{G_{Ic}^m}{G_{Ic}^m} - 1\right)\left(\frac{G_{IIc}^m}{G_{IIc}^m} - 1\right) - \left[\kappa + \varphi\left(\frac{G_{Ic}^m}{G_{Ic}^m + G_{IIc}^m}\right)\right]\left(\frac{G_{Ic}^m}{G_{Ic}^m}\right)\left(\frac{G_{IIc}^m}{G_{IIc}^m}\right) = 0 \quad (16)$$

The linear interaction criterion(Eq. 16) can model all the responses of the simpler interaction criterion(Eq. 15), but by adjusting the arbitrary parameter  $\varphi$ , many more responses can be obtained including an increasing mode I with mode II.  $(\kappa, \varphi)$  values of (3,-4) and (4,-3) were suggested for different materials. The linear interaction criterion is a rather complicated implicit function of  $G_{Ic}$  and  $G_{IIc}$  which could make this criterion difficult to use.

## **BILINEAR FAILURE CRITERION**

The delamination fracture surfaces indicated that a change in failure mechanism may take place in the epoxy around the 1/1 ratio. The mixed-mode fracture toughness data of the epoxy composites also reach a peak at this ratio. If the failure mechanism does change one might expect different failure criteria to hold in different regions of the mixed-mode diagram. Shifting from one criterion to another could easily result in a peak in the toughness response as observed in the epoxy composite data around the 1/1 mixed-mode ratio. Since the linear criterion(Eq. 7) is simple and has seen widespread use, a reasonable assumption would be that the failure response would be linear in each region. The two regions of both the AS4/3501-6 and IM7/977-2 delamination failure data in Figure 2 do appear rather linear which further supports this assumption. The resulting bilinear failure criterion depends on the arbitrary parameters  $\xi$  and  $\zeta$ , as well as the two pure-mode toughnesses.

$$G_{Ic}^m = \xi G_{IIc}^m + G_{Ic} \quad (17)$$

$$G_{Ic}^m = \zeta G_{IIc}^m - \zeta G_{IIc}$$

$\xi$  and  $\zeta$  are the slopes of the two line segments used in the bilinear criterion(Eq. 17). As shown in Figure 16, this criterion can model concave or convex responses, and it can model an increasing mode I fracture toughness component with mode II. If  $\xi=\zeta=-G_{Ic}/G_{IIc}$ , then the bilinear criterion(Eq. 17) would reduce to the linear criterion(Eq. 7)

## CRITERION EVALUATION

The fact that so many radically different mixed-mode criteria have been suggested and used indicate that there is still much to be understood about this phenomenon. The true test of a failure criterion is how well it models the response of the material of interest. In the past, there was no good way to evaluate these criteria. Little mixed-mode data was available, and that which was available was often obtained from several different tests and was therefore inconsistent. Consistent sets of mixed-mode data for three different materials were presented in Figure 2. These data sets will be used to evaluate the different criteria.

Each criterion that produced a general shape close to that of one of the material responses was fit to the data. A least squares analysis was performed to optimize the curve fits. The least squares analysis was conducted by minimizing the distance between each data point and the failure curve. The shapes of the failure curves produced by the  $G_{Ic}$ ,  $G_{IIc}$ ,  $G_{Tc}$  criteria(Eqs. 4, 5, & 6) are not even close to the material responses observed so no attempt was made to fit these criteria to the experimental data. Since the shape of the linear criterion(Eq. 7) was only close to the shape of PEEK data, no attempt was made to use this criterion for either of the epoxies. The power law criterion(Eq. 8) was fit to each material response even though it cannot model the increasing  $G_{Ic}^m$  with  $G_{IIc}^m$  observed in the epoxy composite data.

The increase in  $G_{Ic}^m$  was not that large, and failing to model this increase would at least produce a conservative model for the material. The polynomial, the  $K_{Ic}$ , the hackle, and the COD criteria(Eqs. 9, 10, 11, & 14) were not able to model a material response similar to that seen in the experimental data. The exponential hackle, the exponential  $K_{Ic}/K_{IIc}$ , and the bilinear criteria(Eqs. 12, 13, & 17) were used to model all three material responses. The simple interaction criterion(Eq. 15) was not fit to the data because it is a specialized case of the linear interaction criterion(Eq. 16) which was fit to each set of data.

The results of the least square fit of each criterion to the experimental data is given in Table 2. The best fit curves for AS4/3501-6, IM7/977-2, and AS4/PEEK materials response are shown in Figure 17, 18 and 19, respectively. The linear interaction criterion(Eq. 16) shown by the heavy dashed line and the bilinear criterion(Eq. 17) shown by the solid line, appear to model the epoxies better than the other criteria. This is also indicated by the coefficients of variation  $R^2$  given in Table 2. The closer the coefficient is to 1 the better the model fits the data, and as seen in the table, the linear interaction and the bilinear criterion(Eqs. 16 & 17) produced the coefficients closest to 1 for both AS4/3501-6 and IM7/977-2. The power law criterion(Eq. 8) also had a very low  $R^2$  value for the AS4/3501-6 material, but since the curve does not model the rising  $G_{Ic}^m$  with  $G_{IIc}^m$ , the other criteria are believed to be better choices. Both the linear interaction criterion and the bilinear criterion model the epoxy based composites well and with the same number of arbitrary constants. The complexity of the linear interaction criterion(Eq. 16) makes it difficult to work with since it is an implicit function of  $G_{Ic}^m$  and  $G_{IIc}^m$ . The bilinear criterion is based on very simple equations and is therefore easier to use. For this reason the bilinear is believed to be the best choice of failure criteria for these materials.

The PEEK composite was modeled fairly well by all the criteria tested as seen in Figure 19. The coefficients of variation for this material are all about the same, but

they are all noticeably smaller than the coefficients of the other materials because there are fewer experimental points. The power law criterion(Eq. 8) produced the smallest coefficient of variation, but the linear criterion(Eq. 7) produced a curve that was almost as good and with two less independent variables. For this reason, the linear model is believed to be the best failure criterion for this material. Since the bilinear criterion(Eq. 17) contains two extra degrees of freedom, it models the PEEK material slightly better than the linear criterion(Eq. 7) and might be chosen to be consistent with the criterion used for the epoxy composites.

Because the response of the epoxy composites was quite different from that of the PEEK composite, it is clear that no one failure criterion based on just the pure-mode toughnesses will be able to model all materials. Since delaminations will often be subjected to mixed-mode loading and because the mixed-mode failure response cannot be determined from the pure-mode toughnesses, it is important that mixed-mode toughness testing be included during the characterization of a material. Once the mixed-mode response of a material has been determined, the shape of the response can be compared to the different failure criteria presented here. When choosing the best failure criterion for a given material one should consider which criterion has been used for similar materials. Hopefully a standard choice of failure criteria will emerge for different classes of material such as a linear criterion for thermoplastic composites and a bilinear for epoxy composites. When choosing a failure criterion, one should also consider the number of arbitrary variables and whether criterion is in a form which can be easily used. A simpler criterion with fewer variables is preferred if it models the material as well as a more complicated one. After the appropriate failure criterion for the material is chosen, a least squares fit to the experimental data can be performed to optimize any arbitrary constants of the criterion.

## **CONCLUDING REMARKS**

Many delamination failure criteria which predict a wide variety of mixed-mode fracture toughness responses have been reported in the literature, but few consistent sets of mixed-mode data exist with which to compare these criteria. The MMB test was used to measure the mixed-mode delamination toughness of three different classes of material. A common brittle graphite/epoxy composite (AS4/3501-6), a state of the art toughened graphite/epoxy composite (IM7/977-2), and a tough graphite/thermoplastic composite (AS4/PEEK) were tested. The MMB test is a combination of the pure mode I, DCB test and the pure mode II, ENF test, and can measure fracture toughness at virtually any mixed-mode ratio using a single test specimen configuration. The toughness data are plotted on the mixed-mode diagram ( $G_I$  vs.  $G_{II}$ ). The delamination surfaces were examined and a possible change in failure mechanism was observed in the epoxy composites.

Criteria which have been suggested by other investigators were reviewed and the range of material responses modeled by each criterion were explored. A new bilinear failure criterion was also developed in an attempt to model the possible change in failure mechanism observed in the epoxy composites. The different criteria were compared to the failure response of the three materials tested. The new bilinear failure criterion was considered the best choice for the two graphite/epoxy composites because it modeled the material responses well and because it is relatively simple. The AS4/PEEK composite, which did not show signs of a changing failure mode, was modeled well with either the bilinear or a simpler linear criterion.

Since the response of the epoxy composites was quite different from that of the PEEK composite, it is clear that no one failure criterion based on just the pure-mode toughnesses will be able to model all materials. Because delaminations will often be subjected to mixed-mode loading and because the mixed-mode failure response cannot be determined from the pure-mode toughnesses, it is important that mixed-mode toughness testing be included during the characterization of a material. Once mixed-

mode toughness testing has been conducted the evaluation of the different failure criteria provided in this paper should provide general guidance for selecting an appropriate failure criterion.

## REFERENCES

1. Johnson, W. S., and Mangalgiri, P. D., "Influence on the Resin on Interlaminar Mixed-Mode Fracture," Toughened Composites, ASTM STP 937, Norman J. Johnston, Ed., American Society for Testing and Materials, Philadelphia, PA, 1987, pp. 295-315.
2. Reeder, J. R., and Crews, J. H., Jr., "The Mixed-Mode Bending Method for Delamination Testing," *AIAA Journal*, Vol. 28, No. 7, July 1990, pp. 1270-1276.
3. Reeder, J. R., and Crews, J. H., Jr., "Redesign of the Mixed-Mode Bending Test for Delamination Toughness," Composites Design, Manufacture, and Application, ICCM/8 Conference Proceedings, SAMPE, July 1991, Stephen W. Tsai and George S. Springer, Ed., pp. 36-B-1 - 36-B-10.
4. O'Brien, T. K., Murri, G. B., and Salpekar, S. A., "Interlaminar Shear Fracture Toughness and Fatigue Thresholds for Composite Materials," Composite Materials: Fatigue and Fracture, Second Volume, ASTM STP 1012, Paul A. Lagace, Ed., American Society for Testing and Materials, Philadelphia, 1989, pp. 222-250.
5. Hercules Composites Products Group, "Hercules Prepreg Tape Materials Characterization Data Package," Hercules Co., Magna, Utah, February 1989.
6. Smith, Donald L., and Dow, Marvin B., "Properties of Three Graphite/Toughened Resin Composites," NASA TP3102, September 1991.
7. Murri, G. B., and Martin, R. H., "Effect of Initial Delamination on Mode I and Mode II Interlaminar Fracture Toughness and Fatigue Fracture Threshold," NASA TM 104079, May 1991.
8. Crews, J. H., Jr., and Reeder, J. R., "A Mixed-Mode Bending Apparatus for Delamination Testing," NASA TM 100662, August 1988.
9. Hibbs, M. F., Tse, M. K., and Bradley, W. L., "Interlaminar Fracture Toughness and Real-Time Fracture Mechanism of Some Toughened Graphite/Epoxy Composites," Toughened Composites, ASTM STP 937, Norman J. Johnston, Ed., American Society for Testing and Materials, Philadelphia, 1987, pp. 115-130.
10. Donaldson, S. L., "Fracture Toughness Testing of Graphite/Epoxy and Graphite/PEEK Composites," *Composites*, April 1985, pp.103-109.
11. Morris G. E., "Determining Fracture Directions and Fracture Origins on Failed Graphite/Epoxy Surfaces," Nondestructive Evaluation and Flaw Criticality for Composite Materials, ASTM STP 696, R. B. Pipes, Ed., American Society for Testing and Materials, 1979, pp. 274-297.
12. Whitcomb, J. D., "Analysis of Instability-Related Growth of a Through-Width Delamination," NASA TM 86301, September 1984.
13. Gillespie, J. W., Jr.; Carlsson, L. A.; Pipes, B. R.; Rothschilds, R.; Trethewey, B., and Smiley, A., "Delamination Growth in Composite Materials," NASA CR 176416, December, 1985.
14. Wu, E. M.; and Reuter Jr. R. C.: "Crack extension in fiberglass reinforced plastics" T & AM Report No. 275, University of Illinois, 1965.

15. Spencer, B., and Barnby, J. T., "The Effects of Notch and Fibre Angles on Crack Propagation in Fibre-Reinforced Polymers," *Journal of Material Science*, Vol. 11, 1976, pp. 83-88.
16. Jurf, R. A., and Pipes, R. B., "Interlaminar Fracture of Composite Materials," *Journal of Composite Materials*, Vol. 16, September 1982, pp.386-394.
17. Mall, S., and Kochhar, N. K., "Criterion for Mixed-Mode Fracture in Composite Bonded Joints," NASA CR 178112, May 1986.
18. Ashizawa, M., "Faster interlaminar fracture of a compressively loaded composite containing a defect," Paper presented at the Fifth DOD/NASA Conference on Fibrous Composites in Structural Design, New Orleans, LA, Jan. 1981. (Available as Douglas Paper No. 6994.)
19. Donaldson, S. L., "The Effect of Interlaminar Fracture Properties on the Delamination Buckling of Composite Laminates," *Composite Science and Technology*, Vol. 28, 1987, pp. 33-44.
20. Hashemi, S., Kinloch, A. J., and Williams, J. G., "Mechanics and Mechanisms of Delamination in a Poly(ether sulphone)-Fibre Composite," *Composites Science and Technology*, Vol. 37, 1990, pp. 429-462.
21. Yan, X. Q., Du, S. Y., and Wang, D., "An Engineering Method of Determining The Delamination Fracture Toughness of Composite Laminates," *Engineering Fracture Mechanics*, Vol. 39, No. 4, 1991, pp 623-627.
22. Hahn, H. T., "A Mixed-Mode Fracture Criterion for Composite Materials," *Composites Technology Review*, Vol. 5, Spring, 1983, p. 26-29.
23. Hahn, H. T., and Johannesson, T., "A Correlation Between Fracture Energy and Fracture Morphology in Mixed-Mode Fracture of Composites," *ICM 4*, Vol. 1, 1983, pp. 431-438.
24. White, Scott, R., "Mixed-Mode Interlaminar Fracture of Graphite/Epoxy Composites," Master Thesis, Washington University, Saint Louis, Missouri, May, 1987.
25. Hashemi, S., Kinloch, A. J., and Williams, J. G., "Interlaminar Fracture of Composite Materials," 6th ICCM & 2nd ECCM Conference Proceedings, Elsevier Applied Science, London, Vol. 3, July 1987, pp. 3.254-3.264.
26. Williams, J. G., "The Fracture Mechanics of Delamination Tests," *Journal of Strain Analysis*, Vol. 24, No 4, 1989.
27. Hashemi, S., Kinloch, A. J., and Williams, J. G., "The Effects of Geometry, Rate and Temperature on the Mode I, Mode II and Mixed-Mode I/II Interlaminar Fracture of Carbon-Fibre/ Poly(ether-ether ketone) Composite," *Journal of Composite Materials*, Vol. 24, September 1990, pp. 918-956.
28. Hashemi, S., Kinloch, A. J., and Williams, G., "Mixed-Mode Fracture in Fiber-Polymer Composite Laminates," Composite Materials: Fatigue and Fracture, Vol. 3, ASTM STP 1110, T. K. O'Brien, Ed., American Society for Testing and Materials, Philadelphia, 1991, pp. 143-168.

## APPENDIX A

### LEVER WEIGHT CORRECTION FOR THE MMB TEST

The MMB test uses a lever to apply mode I and mode II loading to the split beam specimen using only one applied load,  $P_a$ . As shown in Figure A1, a gravity load,  $P_g$ , also acts on the lever at a point determined by length  $c_g$ , and this load also contributes to the mode I and mode II loading of the test specimen.

The mode I and mode II loading were given in Reference 2 as

$$P_I = P_a \left( \frac{3c - L}{4L} \right)$$

$$P_{II} = P_a \left( \frac{c + L}{L} \right) \quad (A1)$$

but these equations did not account for the weight of the lever. The weight of the lever can be thought of as a second applied load which is superimposed on the true applied loading. The mode I and mode II loadings are therefore given by

$$P_I = P_a \left( \frac{3c - L}{4L} \right) + P_g \left( \frac{3c_g - L}{4L} \right)$$

$$P_{II} = P_a \left( \frac{c + L}{L} \right) + P_g \left( \frac{c_g + L}{L} \right) \quad (A2)$$

The equations for mode I and mode II strain energy release rate are given by Equations A3.

$$G_I = \frac{P_I^2}{bE_{11}I} \left[ a^2 + \frac{2a}{\lambda} + \frac{1}{\lambda^2} + \frac{h^2 E_{11}}{10G_{13}} \right]$$

$$G_{II} = \frac{3P_{II}^2}{64bE_{11}I} \left[ a^2 + \frac{.2h^2 E_{11}}{G_{13}} \right]$$

where

$$\lambda = \frac{1}{h} \sqrt[4]{\frac{6E_{22}}{E_{11}}}$$

$$I = \frac{bh^3}{12} \quad (A3)$$

Substituting Eq. A2 into Eq. A3 gives an expression for  $G$  in terms of the applied load and lever weight.

$$\begin{aligned}
G_I &= \left[ \begin{array}{l} (36c^2 - 24cL + 4L^2)P_a^2 + \\ (72cc_g - 24cL - 24c_gL + 8L^2)P_aP_g + \\ (36c_g^2 - 24c_gL + 4L^2)P_g^2 \end{array} \right] \left[ \frac{a^2 + \frac{2a}{\lambda} + \frac{1}{\lambda^2} + \frac{h^2E_{11}}{10G_{13}}}{64L^2bE_{11}I} \right] \\
G_{II} &= \left[ \begin{array}{l} (3c^2 + 6cL + 3L^2)P_a^2 + \\ (6cc_g + 6cL + 6c_gL + 6L^2)P_aP_g + \\ (3c_g^2 + 6c_gL + 3L^2)P_g^2 \end{array} \right] \left[ \frac{a^2 + \frac{.2h^2E_{11}}{G_{13}}}{64L^2bE_{11}I} \right] \quad (A4)
\end{aligned}$$

Notice that since the load is squared in Eq. A3, a cross term develops in Eq. A4 between the applied load and the weight. These equations that account for the weight of the lever are equivalent to the equations for  $G$  given in Reference 2 if the terms involving  $P_g$  are removed.

Eq. A4 has been developed assuming the delamination faces are not in contact. When  $c$  is small ( $c \lesssim 0.67$ ), the delamination faces do not separate and load is transferred across the faces.  $P_I$  (Eq. A2) is the load pulling the delamination open so that a negative  $P_I$  is the load pushing the delamination faces together. If  $P_I$  is negative, the faces are in contact so  $G_I$  will equal zero, but  $G_{II}$  can still be found using Eq. A4.

The errors caused by ignoring the weight of the lever are calculated using Eq. A5.

$$\begin{aligned}
\% \text{ Error } G_I &= \frac{(G_I)_w - (G_I)_o}{(G_I + G_{II})_o} \times 100 \\
\% \text{ Error } G_{II} &= \frac{(G_{II})_w - (G_{II})_o}{(G_I + G_{II})_o} \times 100 \quad (A5)
\end{aligned}$$

The subscripts  $w$  and  $o$  indicate that the lever weight was included or neglected, respectively. The errors are normalized by total strain energy release rate,  $G_I + G_{II}$ , so that a small nominal error in  $G_I$  or  $G_{II}$  does not cause a large apparent error just because that component also happens to be small.

The error caused by ignoring the lever weight of the MMB apparatus used in the present study is presented in Figure A2. The errors in  $G_I$  and  $G_{II}$  are plotted as a function of lever load position for total strain energy release rate values from 0.3 to 3 in-lb/in. The redesigned MMB apparatus used in this study was found to weigh 1.85 lb. The weight is partly due to the saddle mechanism which moves when the lever load point is moved. Since the saddle mechanism is moved when the lever load point is changed, the center of gravity of the lever assembly given by length  $c_g$  also changes. The relationship between  $c$  and  $c_g$  was found for this apparatus to be  $c_g = 0.38 + 0.24 c$ . The  $c$  values that produce the mixed-mode ratios used in this study are also marked on the Figure. For the range of lever lengths tested in this study, the largest error in  $G_I$  was at the 4/1 mixed-mode ratio ( $c=3.83$  in.) and the largest error in  $G_{II}$  was at  $c=0.66$  in. The error in both  $G_I$  and  $G_{II}$  increases rapidly as  $G_I + G_{II}$  goes below 1 in-lb/in<sup>2</sup>, but for  $G_I + G_{II}$  above 2 in-lb/in<sup>2</sup> the error is always below  $\pm 5\%$  which is negligible for this type of testing.

A simple test was developed to determine when the added complexity of accounting for the lever weight is necessary. First Eq. A4 was substituted into Eq. A5. The error calculations were first simplified as shown in Eq. A6 by neglecting the end foundation ( $\lambda=0$ ) and shear correction ( $G_{13}=\infty$ ) terms found in Eq. A4. Higher order term involving  $P_g^2$  were also neglected.

$$\begin{aligned} \% \text{ Error } G_I &\approx \frac{(72cc_g - 24cL - 24c_gL + 8L^2)}{(39c^2 - 18cL + 7L^2)} \frac{P_g}{P_a} \times 100 \\ \% \text{ Error } G_{II} &\approx \frac{(6cc_g + 6cL + 6c_gL + 6L^2)}{(39c^2 - 18cL + 7L^2)} \frac{P_g}{P_a} \times 100 \end{aligned} \quad (\text{A6})$$

Equation A6 is a function of  $P_a$ , but the critical value of  $P_a$  is usually not know before testing.  $P_a$  was replaced by a function of the total strain energy release rate,  $G_I + G_{II}$ . The expression for total strain energy release rate was obtained from Eqs. A4 and simplified by neglecting the correction for lever weight, shear and end foundation

as discussed earlier. Equations for the maximum  $G_I$  and  $G_{II}$  errors were created using the  $c$  values that gave the worst errors in  $G_I$  and  $G_{II}$  as seen in Figure A2. Therefore  $c=3.84$  in. and  $c=.66$  in. were substituted into the  $G_I$  and  $G_{II}$  error equations, respectively. Since the largest  $G_I$  error occurs near the pure mode I condition and the largest  $G_{II}$  error occurs near the pure mode II condition,  $G_{Ic}$  and  $G_{IIc}$  were substituted into the two equations respectively. The resulting estimates of the maximum errors due to lever weight are

$$\begin{aligned} \text{Max \% Error } G_{Ic}^m &\approx 1.3 \left( \frac{c_g}{L} - \frac{1}{3} \right) \frac{aP_g}{\sqrt{G_{Ic} bE_{11} I}} \times 100 \\ \text{Max \% Error } G_{IIc}^m &\approx 0.43 \left( \frac{c_g}{L} + 1 \right) \frac{aP_g}{\sqrt{G_{IIc} bE_{11} I}} \times 100 \end{aligned} \quad (A7)$$

If the maximum error for both mode I and mode II are below say  $\pm 5\%$ , then the weight of the lever can be ignored. If the error is larger than  $\pm 5\%$ , the additional terms in Eq. A4 involving  $P_g$  should be used in calculating  $G$ . If the additional terms are needed at one mixed-mode ratio, they should be used at all mixed-mode ratios tested for that material so that the data is consistent.

Table 1. Material Properties

Material	$E_{11}$ (measured)	$E_{22}$	$G_{13}$
AS4/3501-6	19.1 Msi	1.4 Msi	0.85 Msi
IM7/977-2	20.8 Msi	1.33 Msi	0.694 Msi
AS4/PEEK (APC2)	18.7 Msi	1.46 Msi	0.8 Msi

Table 2. Least Square curve fit parameters for various criteria

Material	Criterion	$G_{Ic}$	$G_{IIc}$	Constants	$R^2$
AS4/3501-6	Power Law(Eq. 8)	.5185	3.990	$\alpha= 0.0571$ $\beta= 5.039$	.9956
	Exponential Hackle(Eq. 12)	.4422	3.713	$\gamma= 0.1964$	.9924
	Exponential K(Eq. 13)	.5172	3.092	$\eta= 1.664$	.9888
	Linear Interaction(Eq. 16)	.4740	4.050	$\kappa= 1.279$ $\varphi=-4.905$	.9960
	Bilinear(Eq. 17)	.4548	3.269	$\xi= 0.2039$ $\zeta= 0.2473$	.9956
IM7/977-2	Power Law(Eq. 8)	1.792	8.635	$\alpha= 0.126$ $\beta= 5.447$	.9960
	Exponential Hackle(Eq. 12)	1.345	8.354	$\gamma= 0.304$	.9962
	Exponential K(Eq. 13)	1.730	7.833	$\eta= 1.050$	.9948
	Linear Interaction(Eq. 16)	1.616	8.557	$\kappa= 0.868$ $\varphi=-2.962$	.9974
	Bilinear(Eq. 17)	1.619	8.106	$\xi= 0.2107$ $\zeta= -0.371$	.9976
AS4/PEEK	Linear(Eq. 7)	4.745	7.147		.9787
	Power Law(Eq. 8)	4.753	6.649	$\alpha= 1.662$ $\beta= 0.7329$	.9811
	Exponential Hackle(Eq. 12)	4.538	6.734	$\gamma= 0.8701$	.9797
	Exponential K(Eq. 13)	4.509	6.733	$\eta= 0.4940$	.9799
	Linear Interaction(Eq. 16)	4.778	6.736	$\kappa= 0.8679$ $\varphi= 1.058$	.9803
	Bilinear(Eq. 17)	4.433	6.861	$\xi= -0.1261$ $\zeta= -0.7477$	.9801

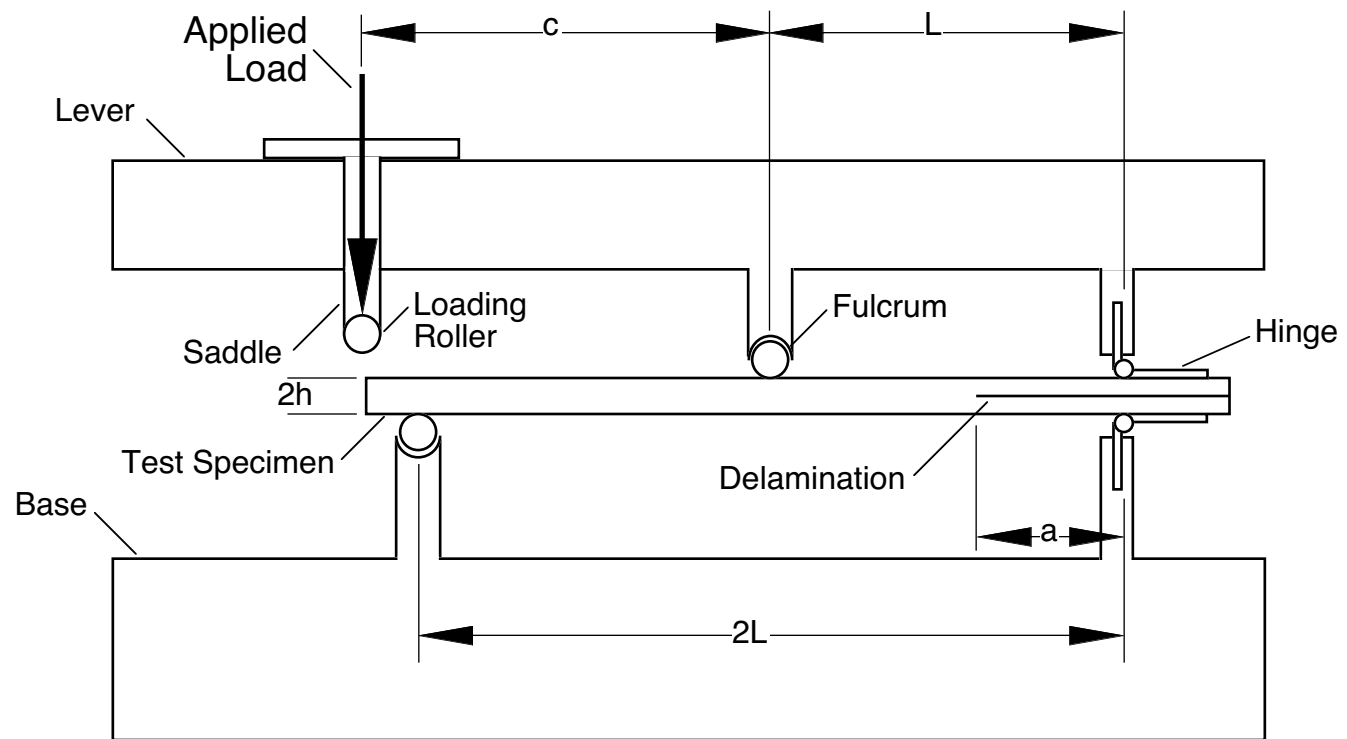


Figure 1. The redesigned mixed-mode bending test apparatus.

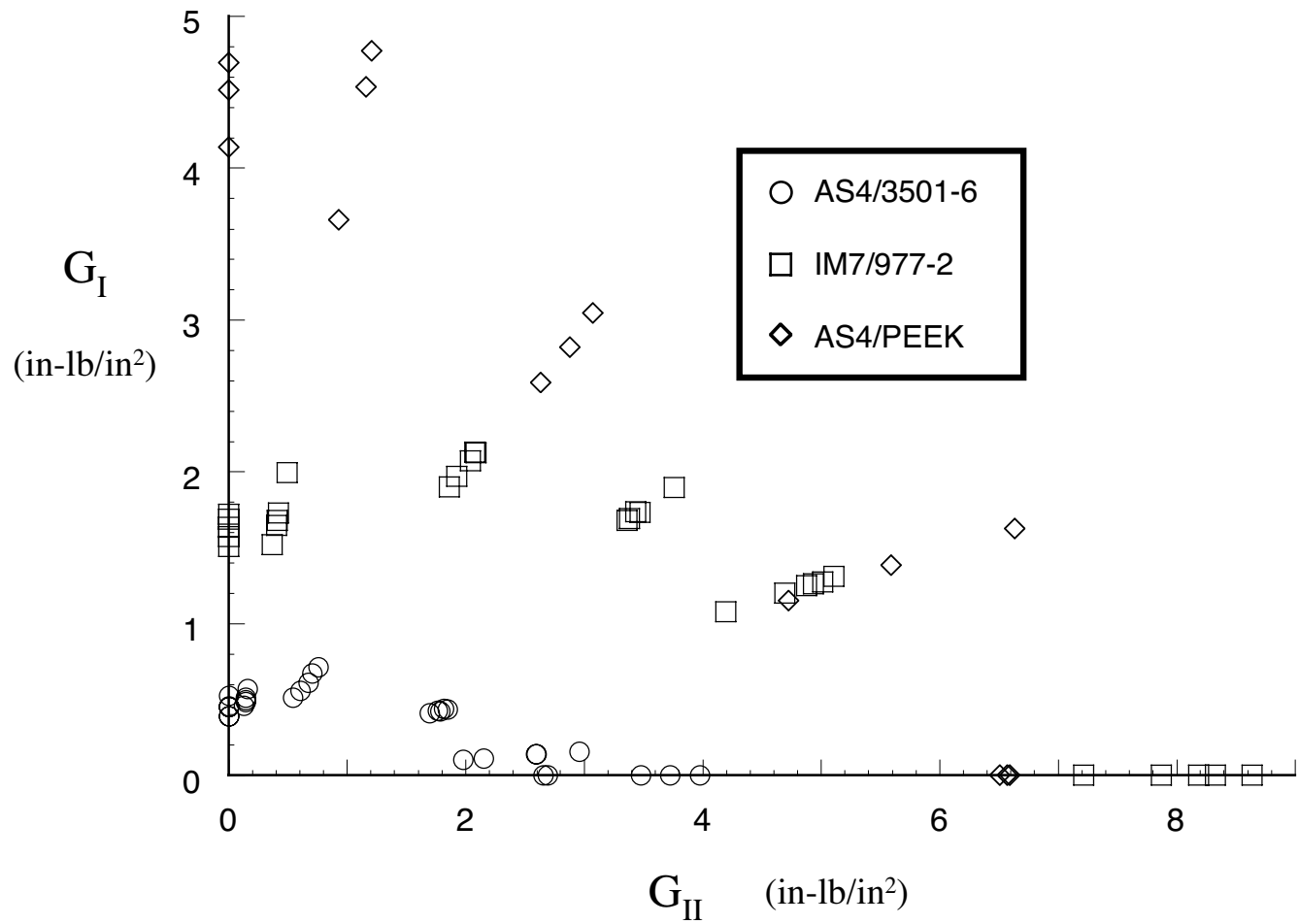


Figure 2. Mixed-mode failure responses of graphite composite materials.

Delamination  
Growth  
↓

32

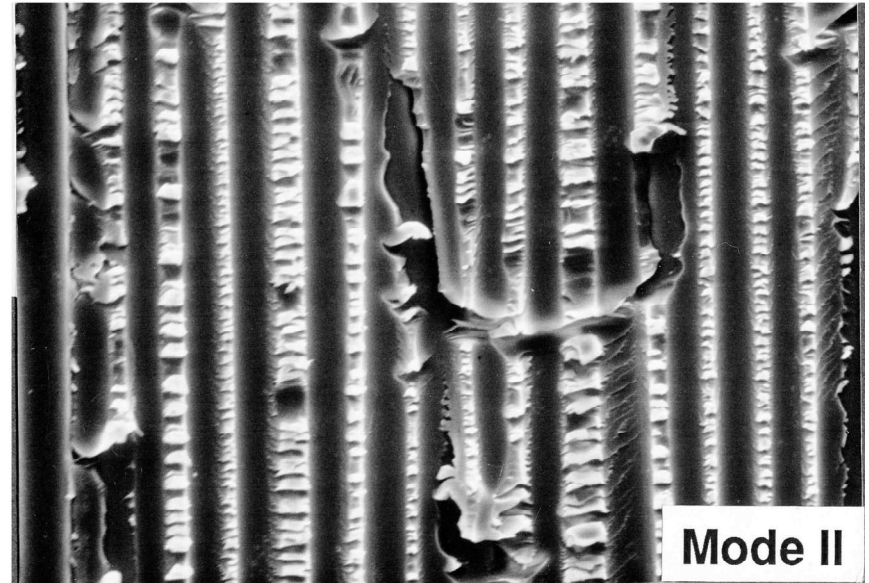
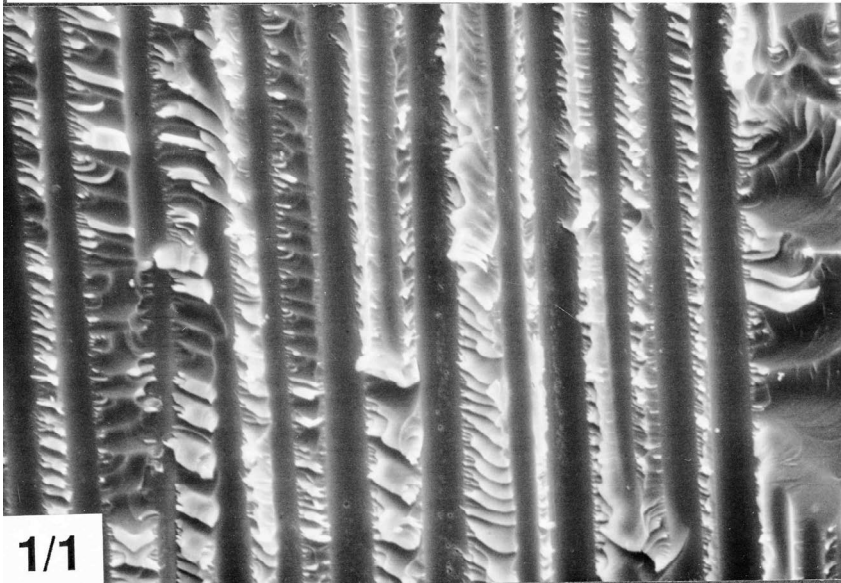
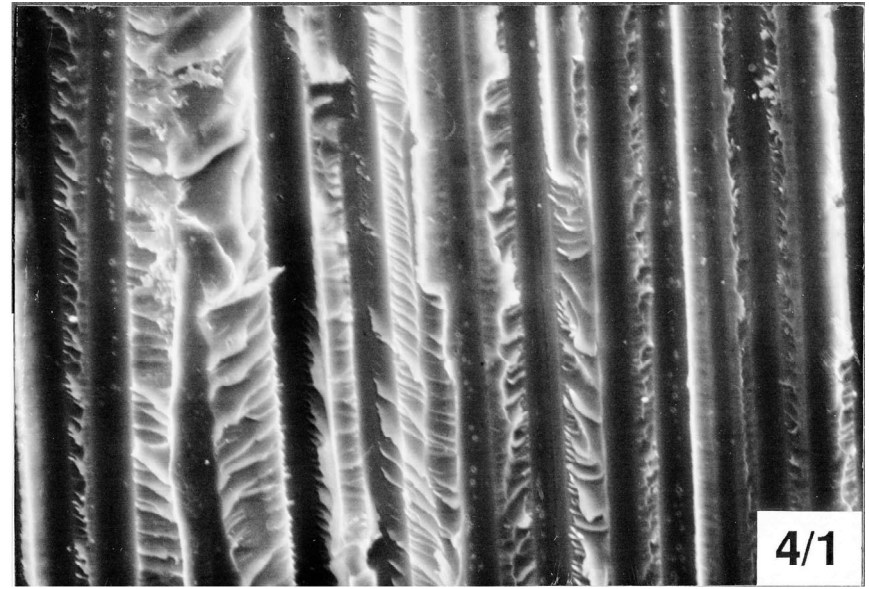
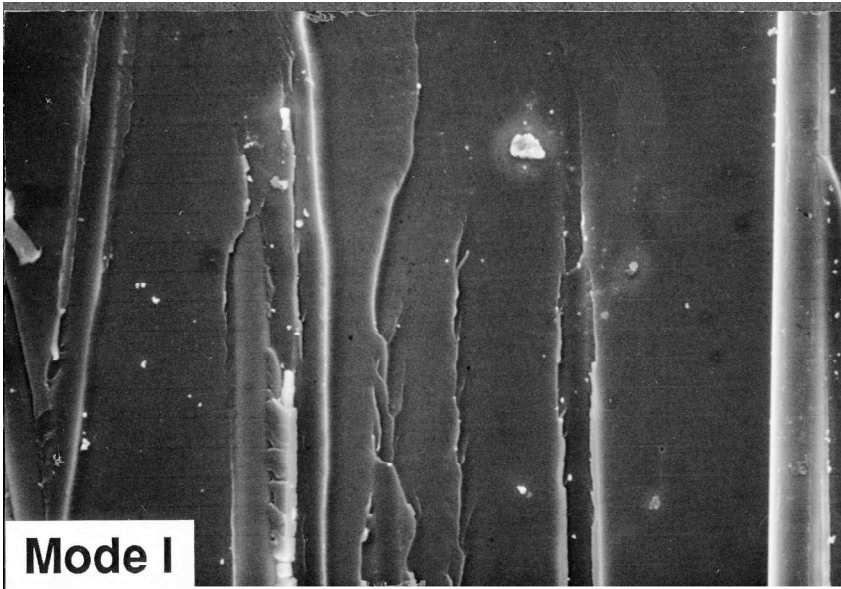


Figure 3. Delamination photomicrographs of AS4/3501-6 at different mixed-mode ratios. (1000x)

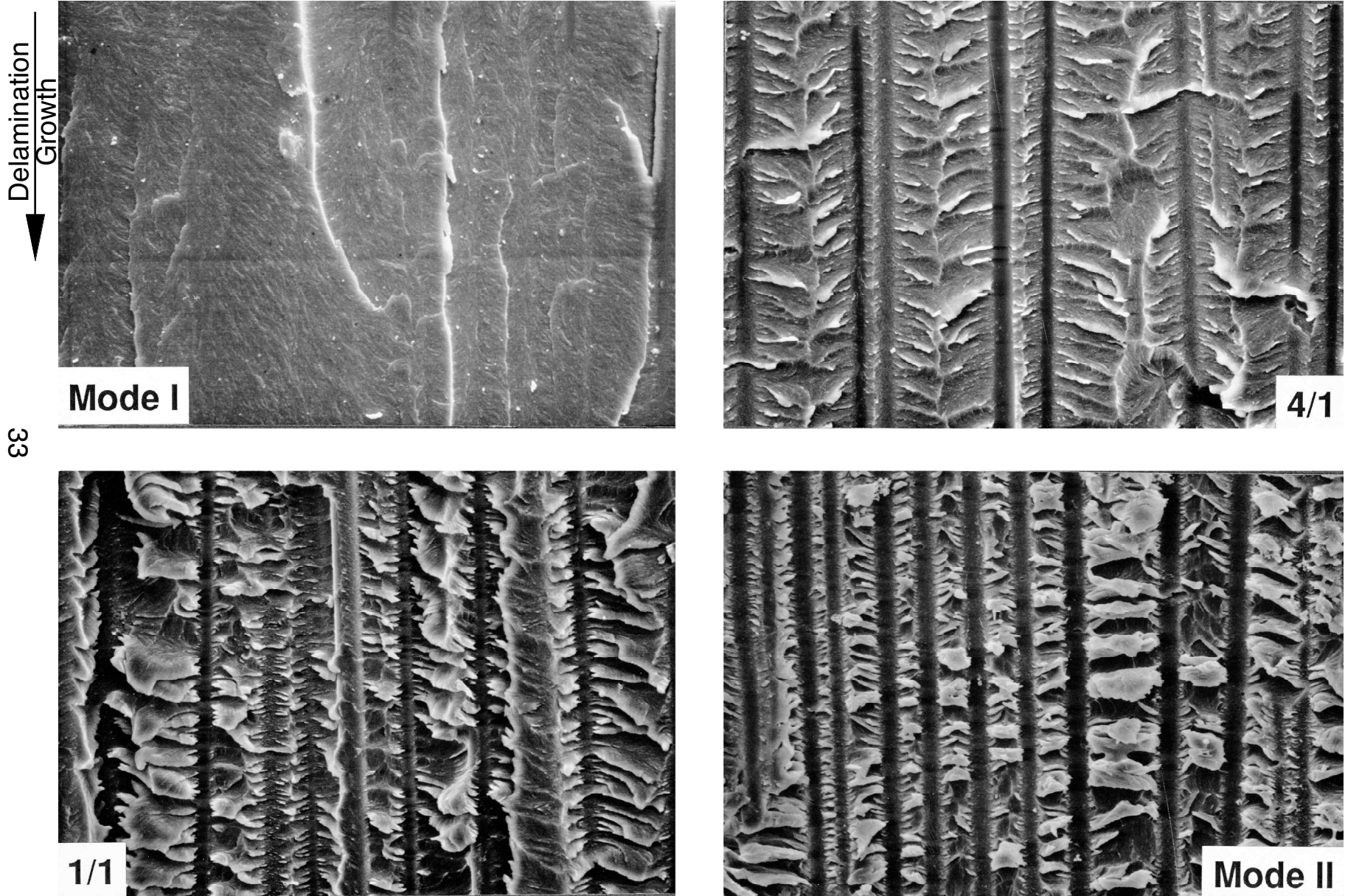


Figure 4. Delamination photomicrographs of IM7/977-2 at different mixed-mode ratios. (1000x)

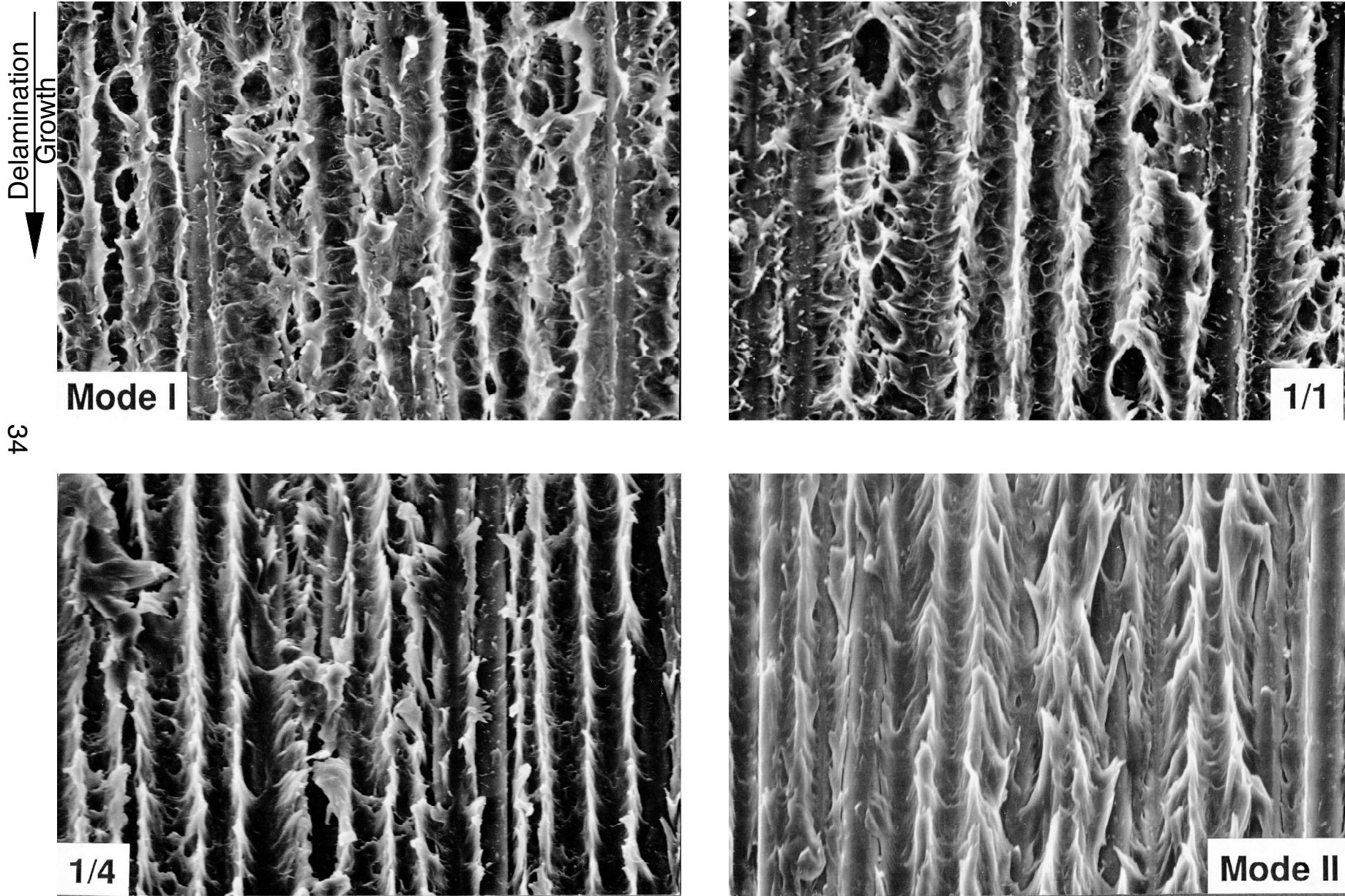


Figure 5. Delamination photomicrographs of AS4/PEEK at different mixed-mode ratios. (1000x)

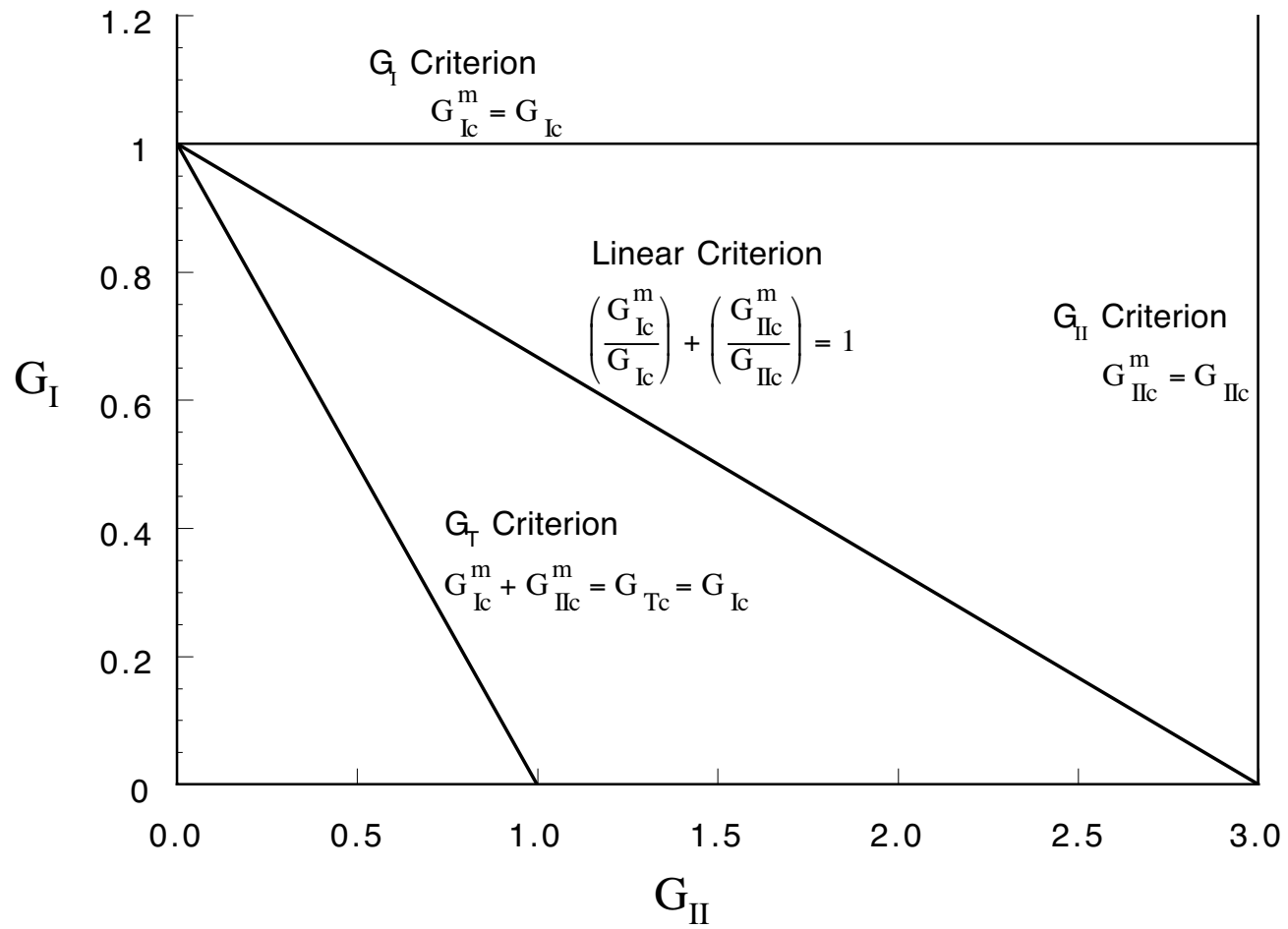


Figure 6. Mixed-mode fracture toughness diagrams for simple criteria.

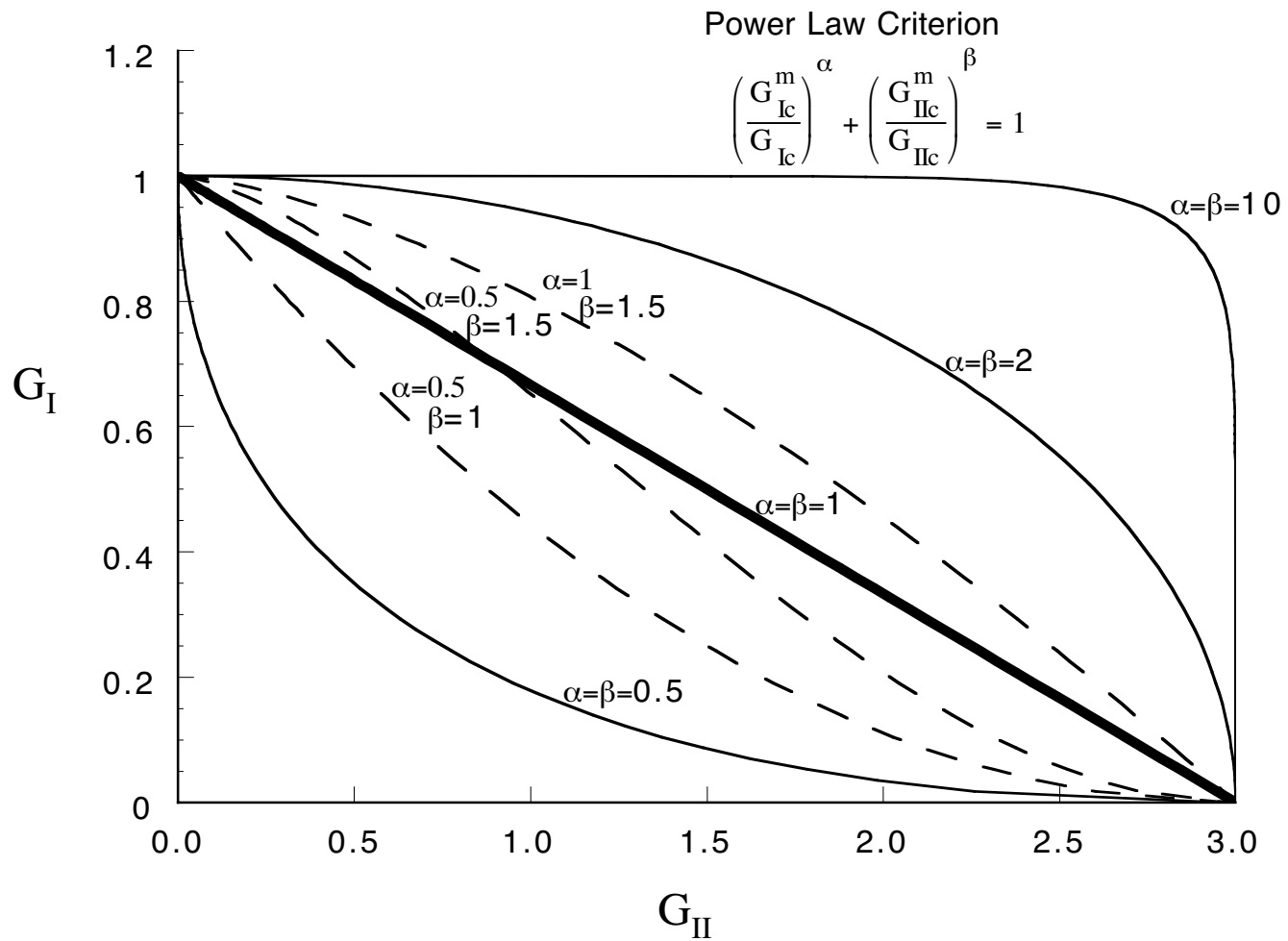


Figure 7. Mixed-mode fracture toughness diagram for the power law criterion(Eq. 8).

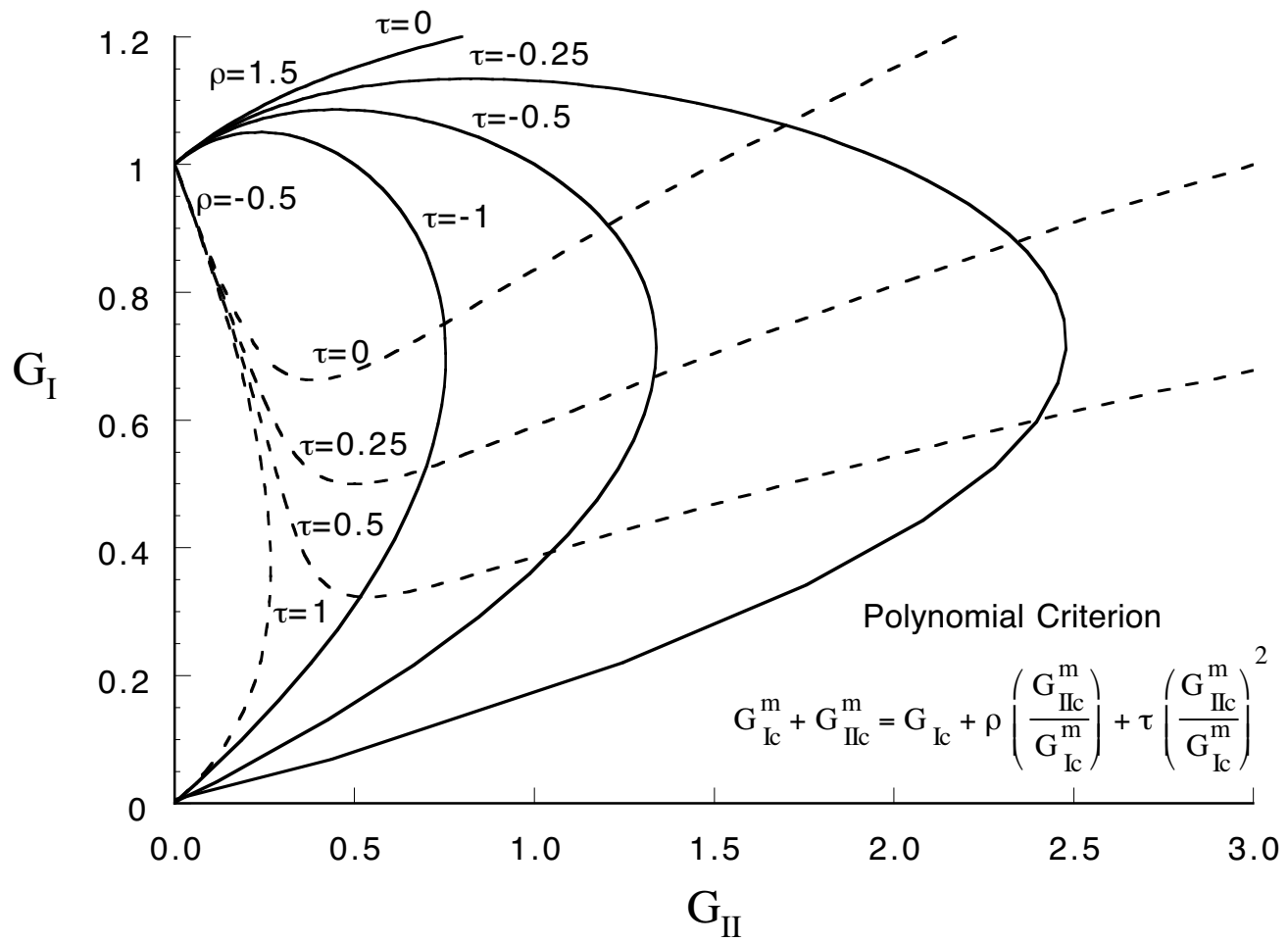


Figure 8. Mixed-mode fracture toughness diagram for the polynomial criterion(Eq. 9).

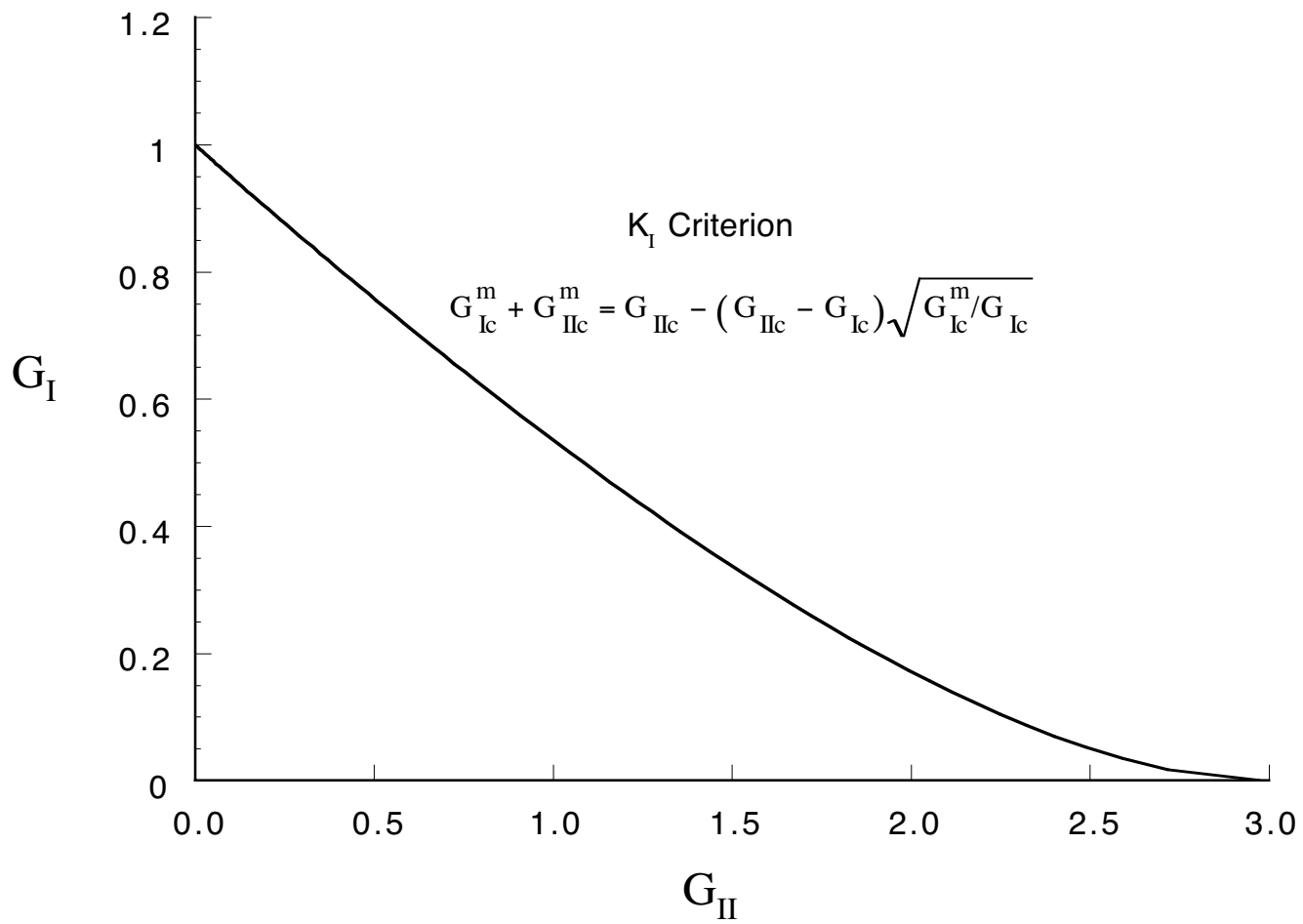


Figure 9. Mixed-mode fracture toughness diagram for the  $K_I$  criterion(Eq. 10).

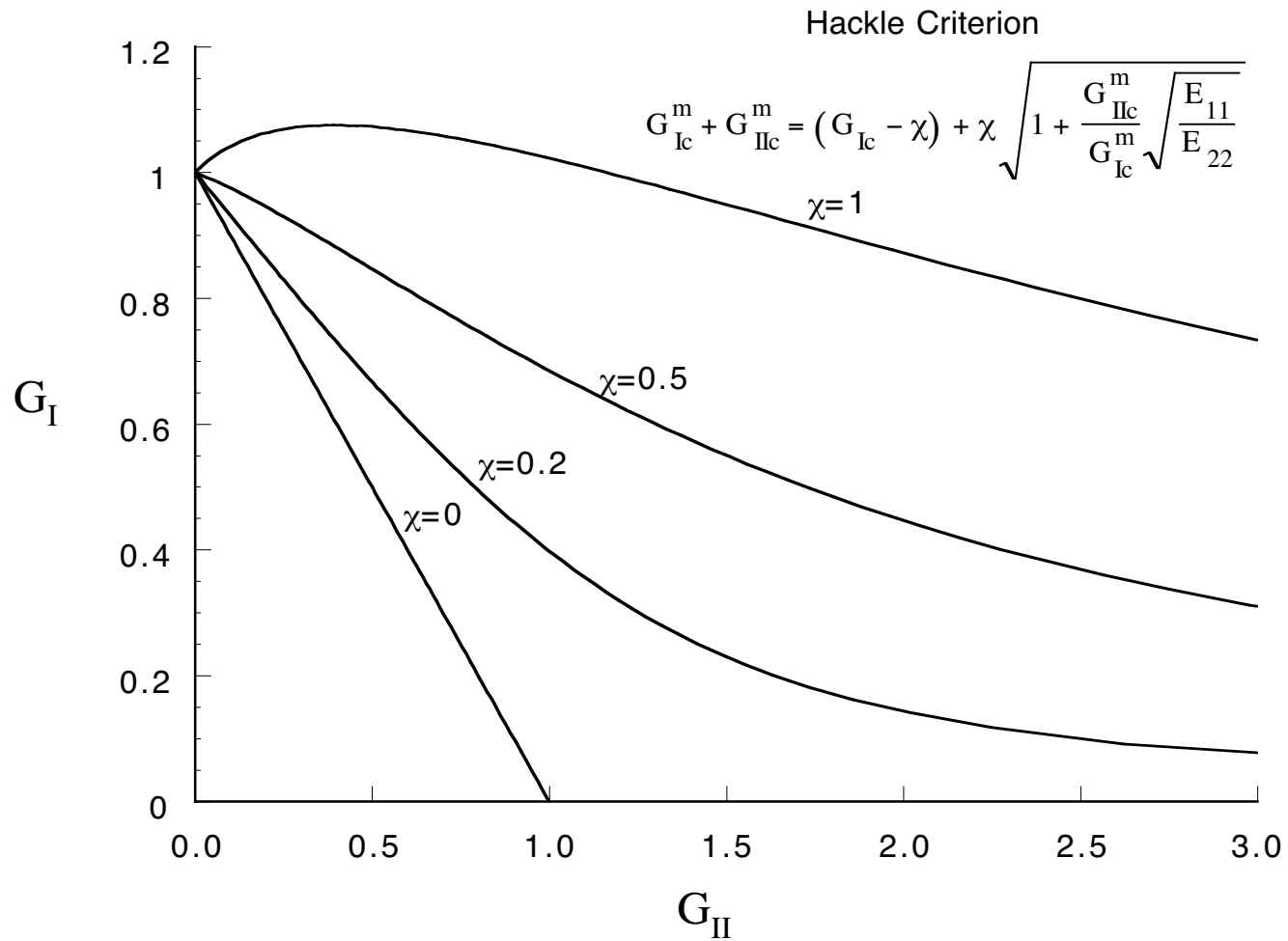


Figure 10. Mixed-mode fracture toughness diagram for the hackle criterion(Eq. 11).

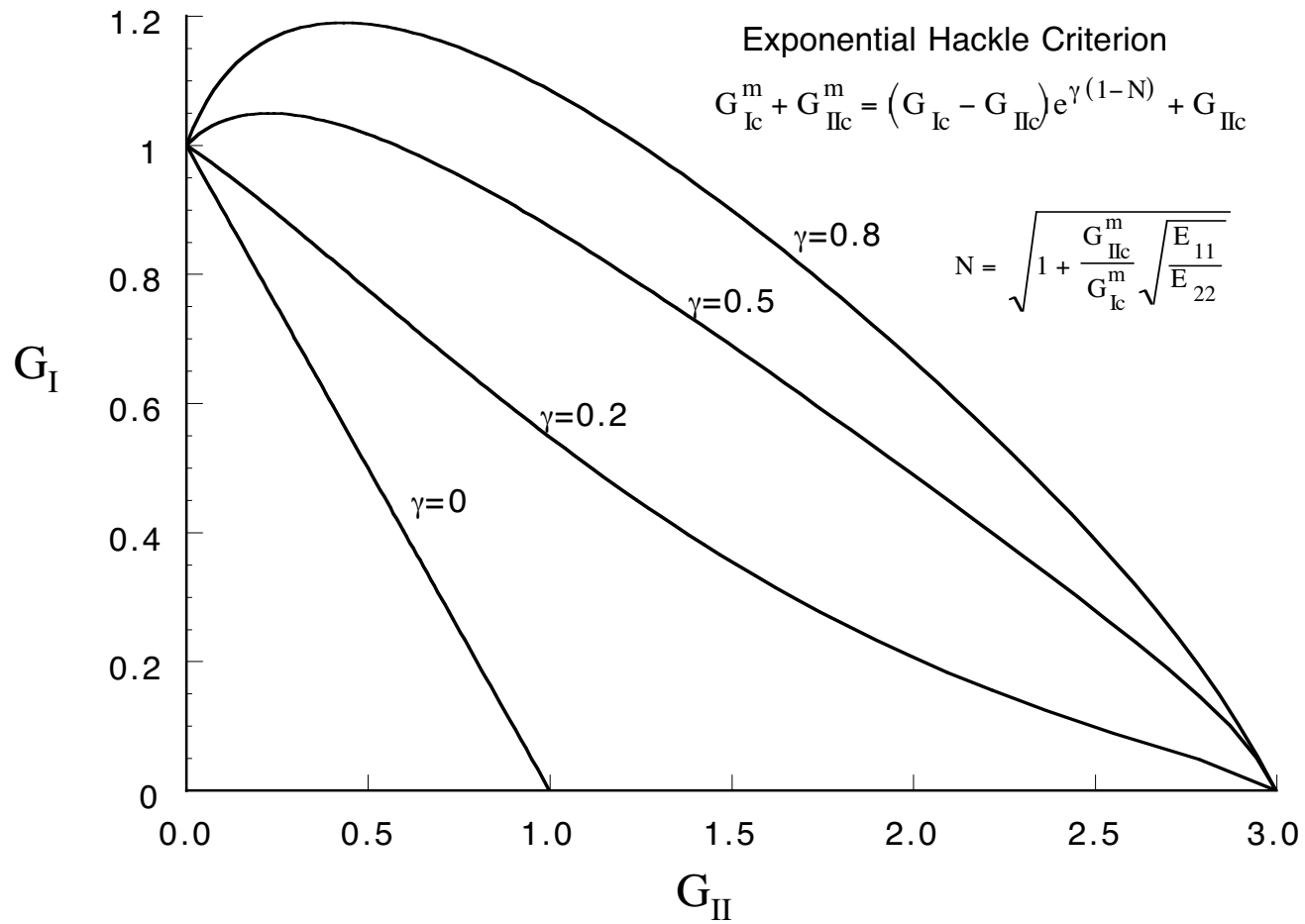


Figure 11. Mixed-mode fracture toughness diagram for the exponential hackle criterion(Eq. 12).

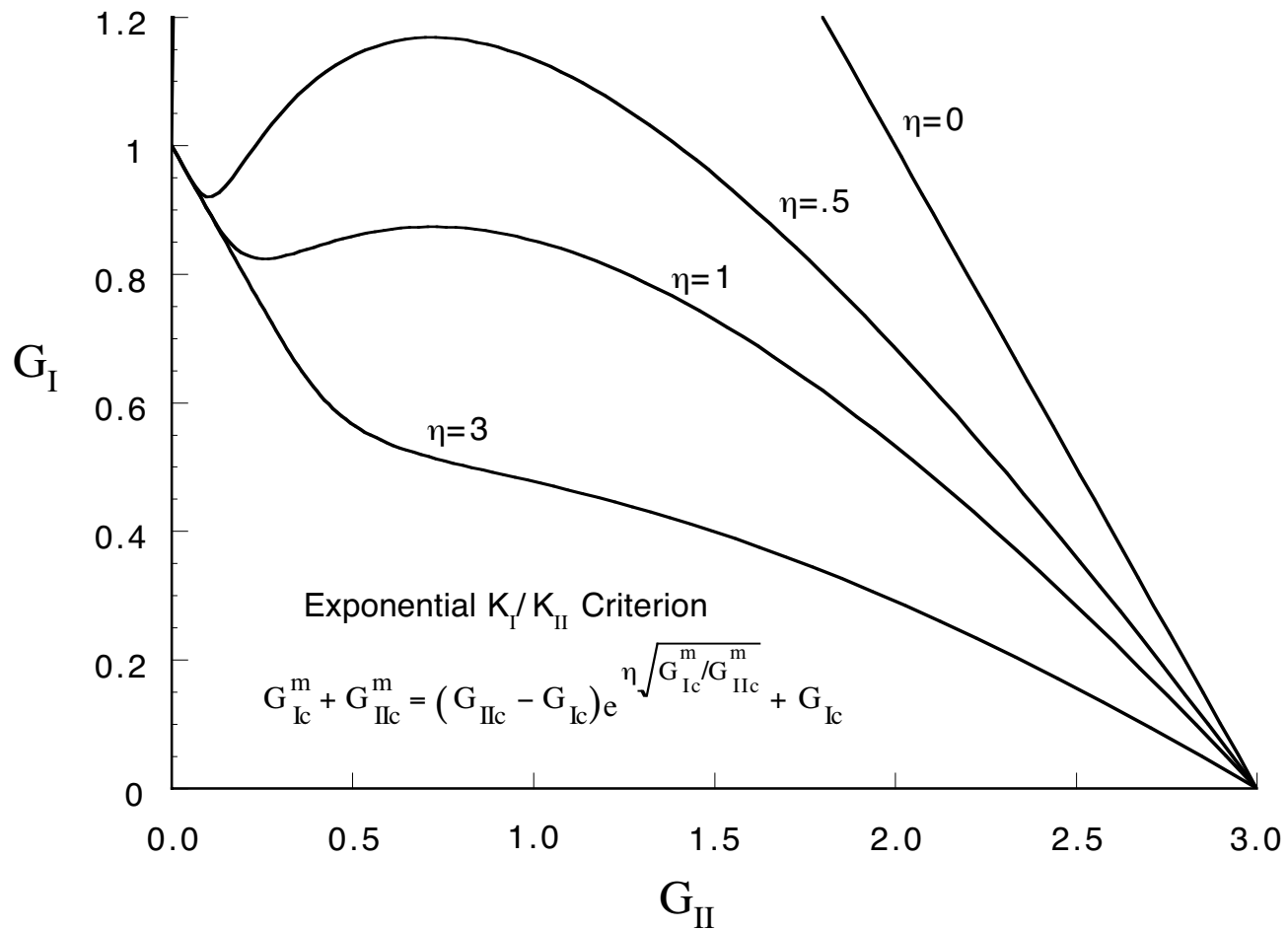


Figure 12. Mixed-mode fracture toughness diagram for the exponential  $K_I/K_{II}$  criterion(Eq. 13).

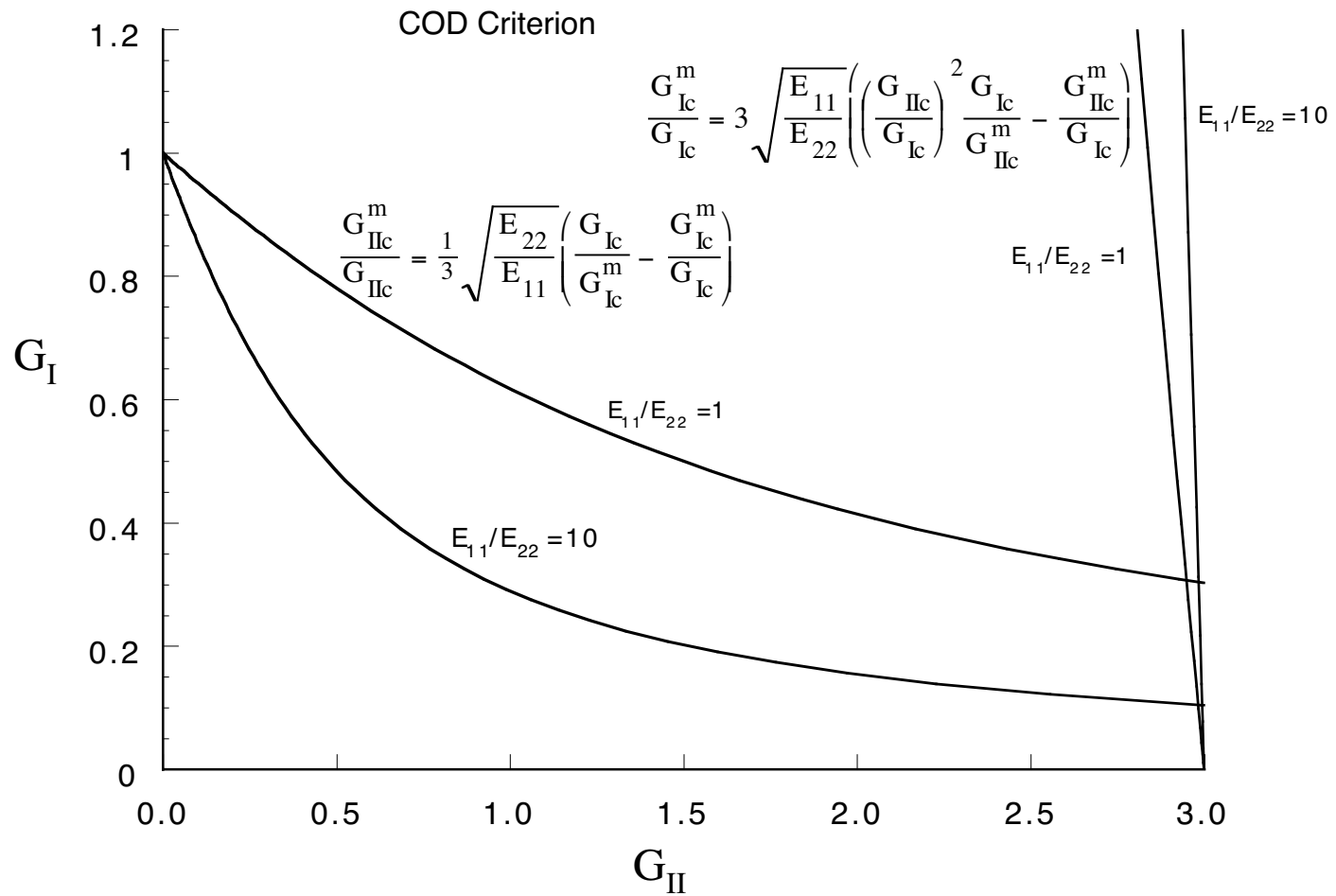


Figure 13. Mixed-mode fracture toughness diagram for the crack opening criterion(Eq. 14).

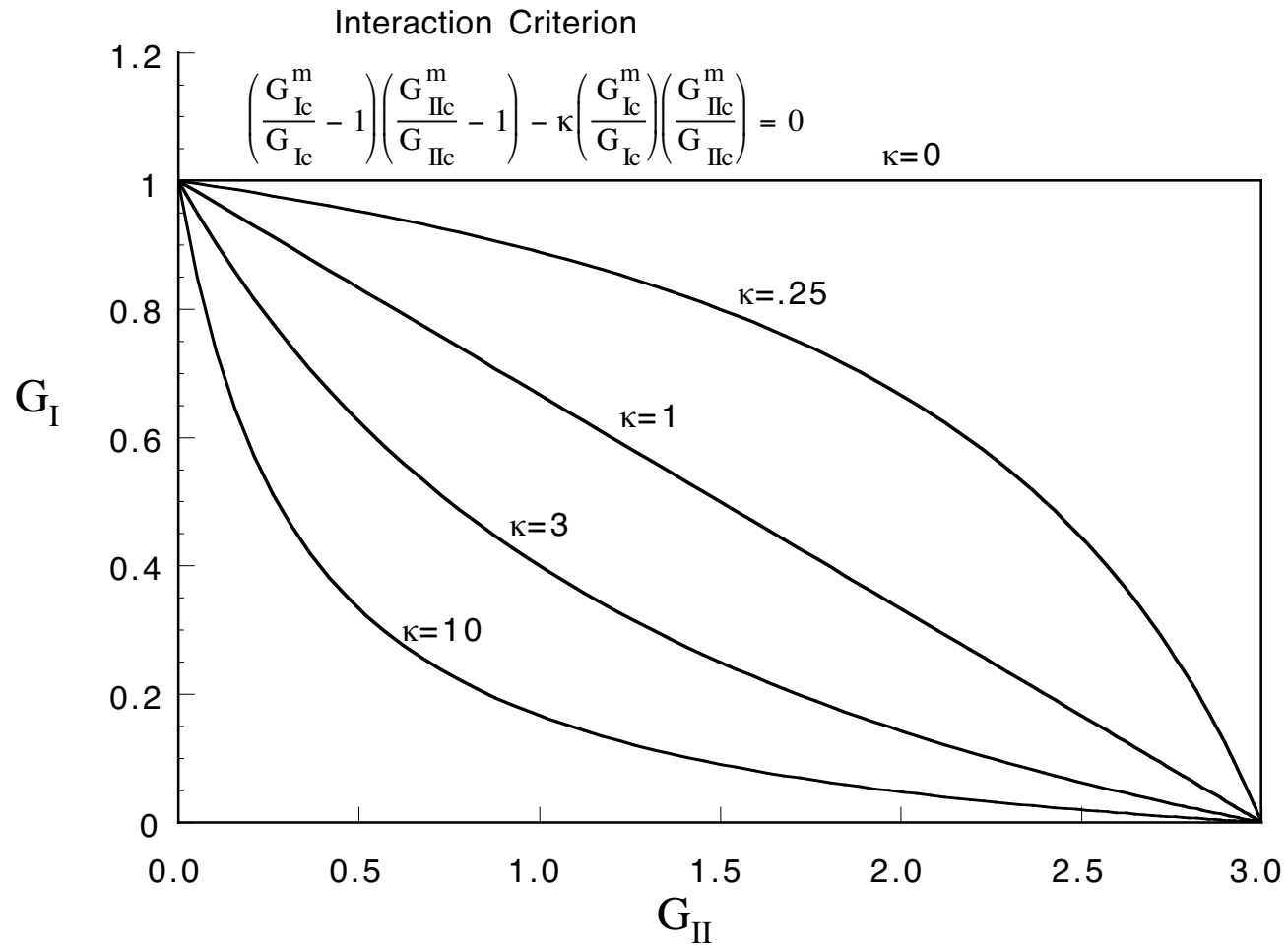


Figure 14. Mixed-mode fracture toughness diagram for the interaction criterion(Eq. 15).

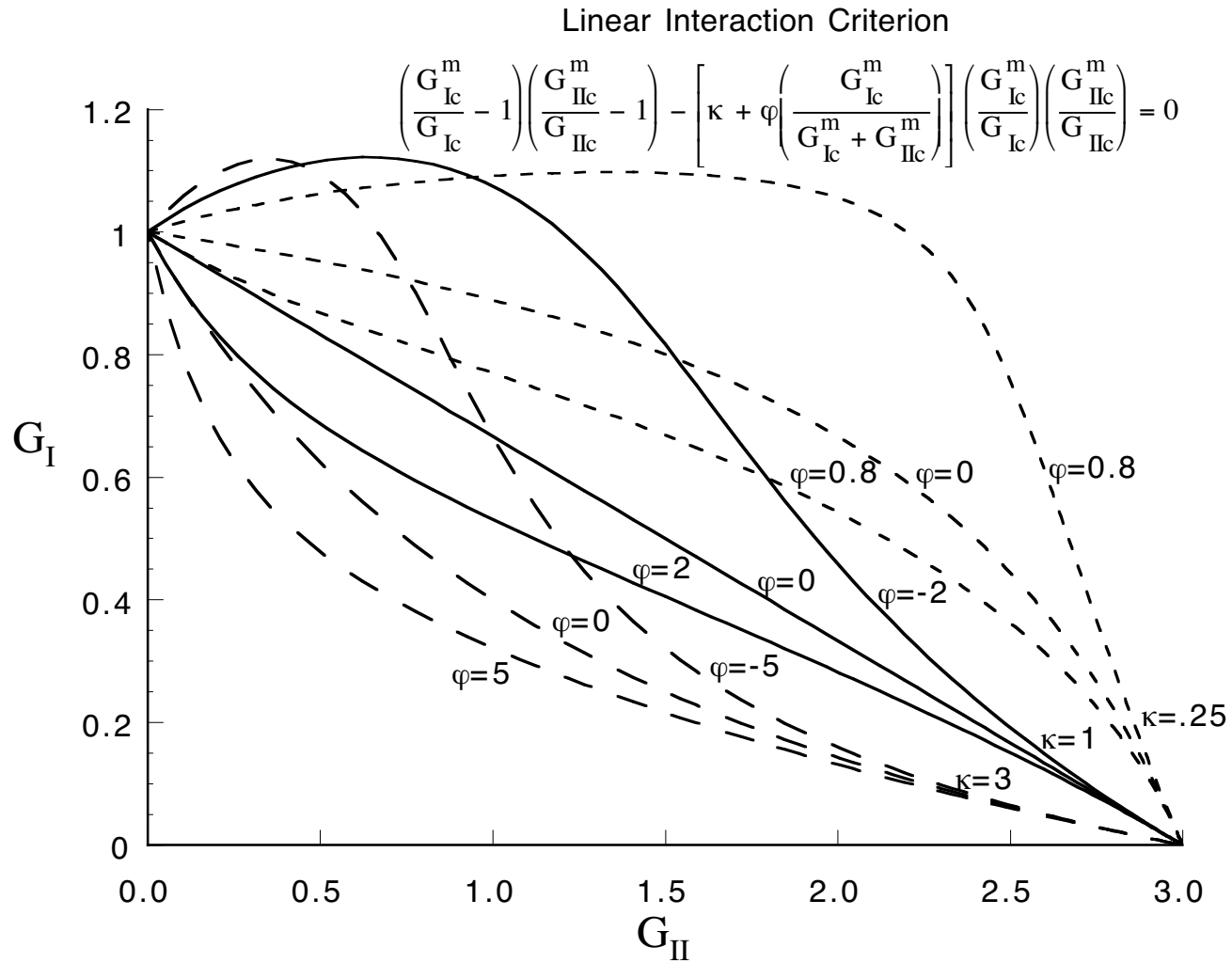


Figure 15. Mixed-mode fracture toughness diagram for the linear interaction criterion(Eq. 16).

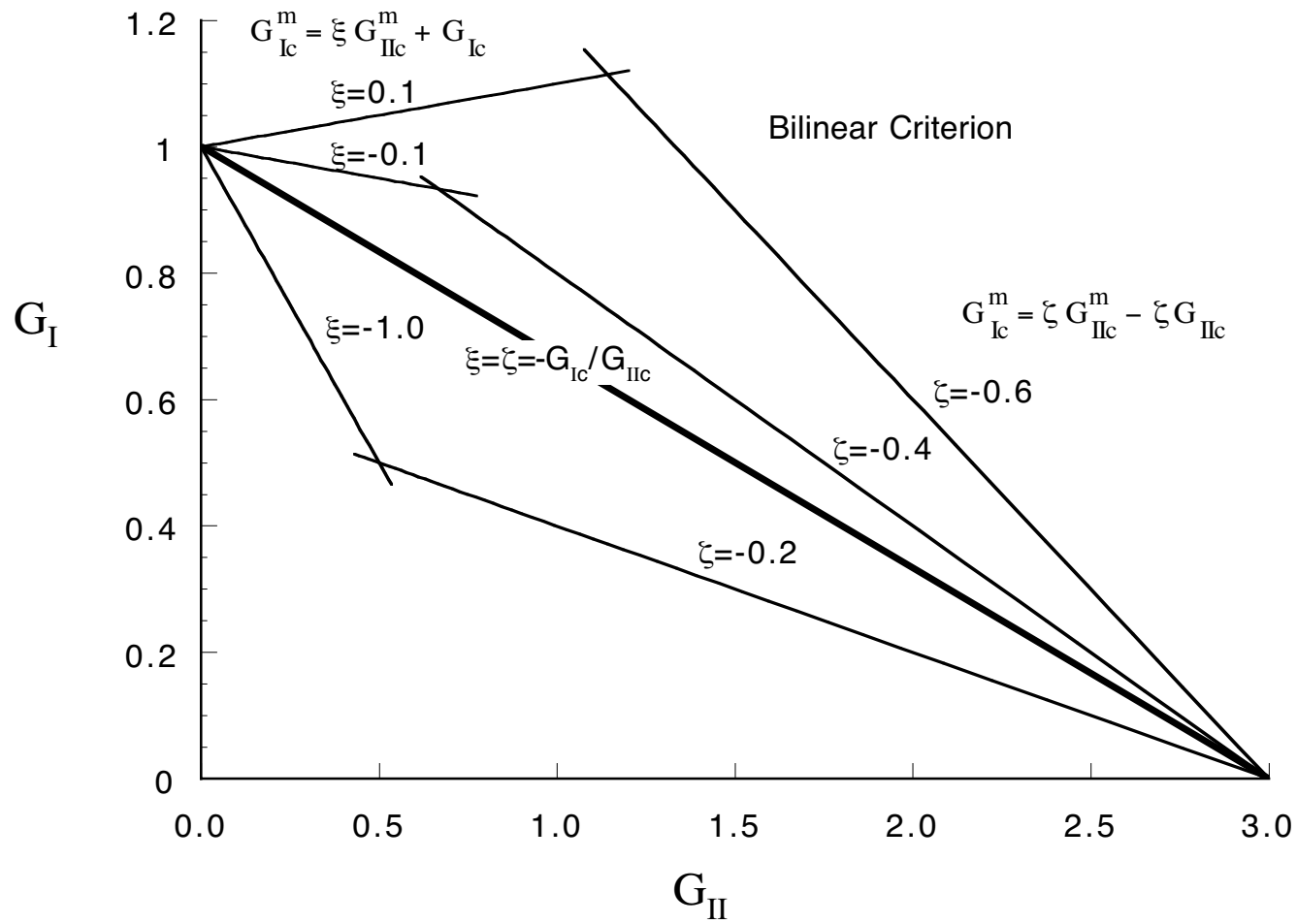


Figure 16. Mixed-mode fracture toughness diagram for the bilinear criterion(Eq. 17).

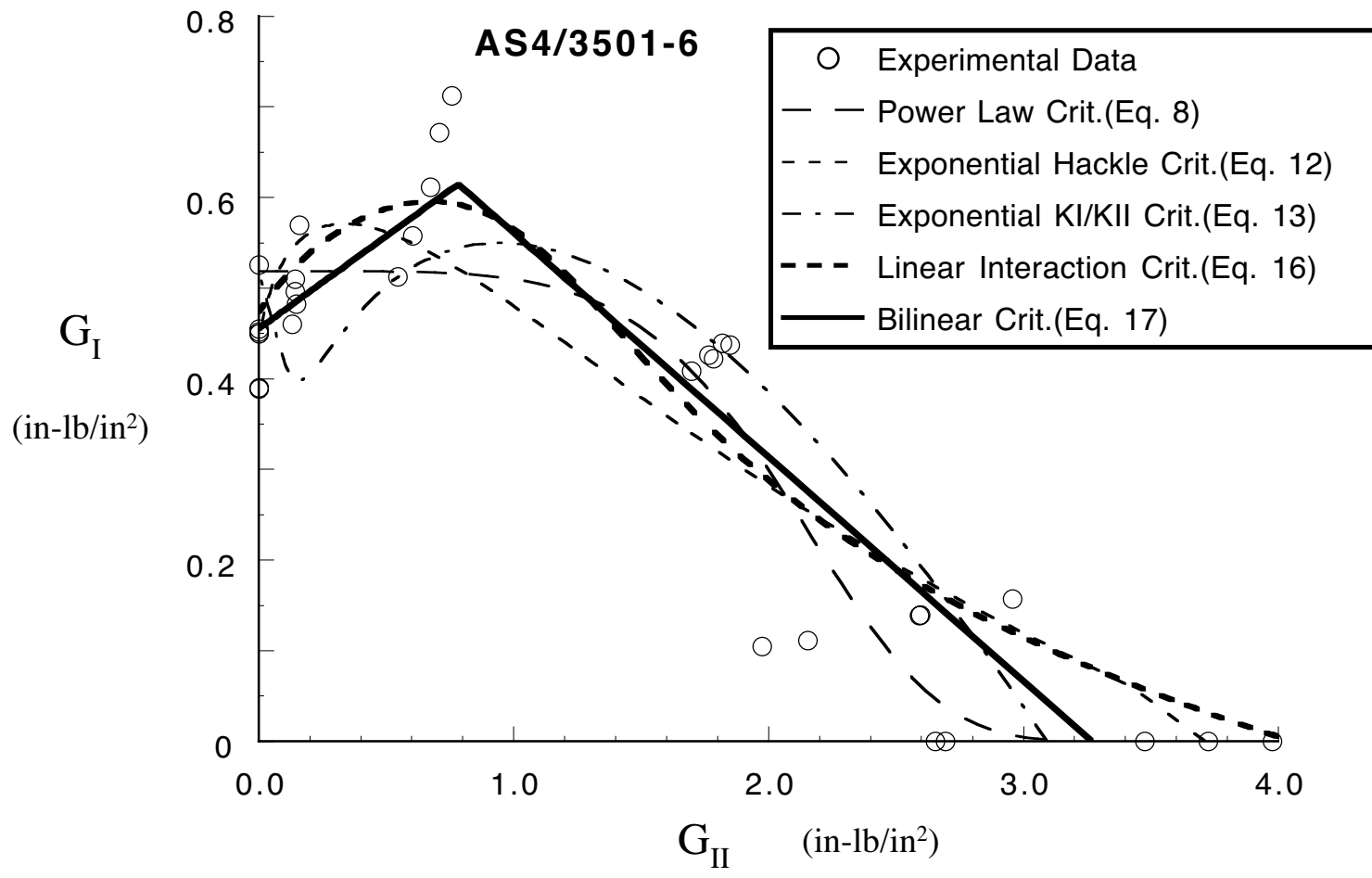


Figure 17. Mixed-mode toughness criterion curves for AS4/3501-6.

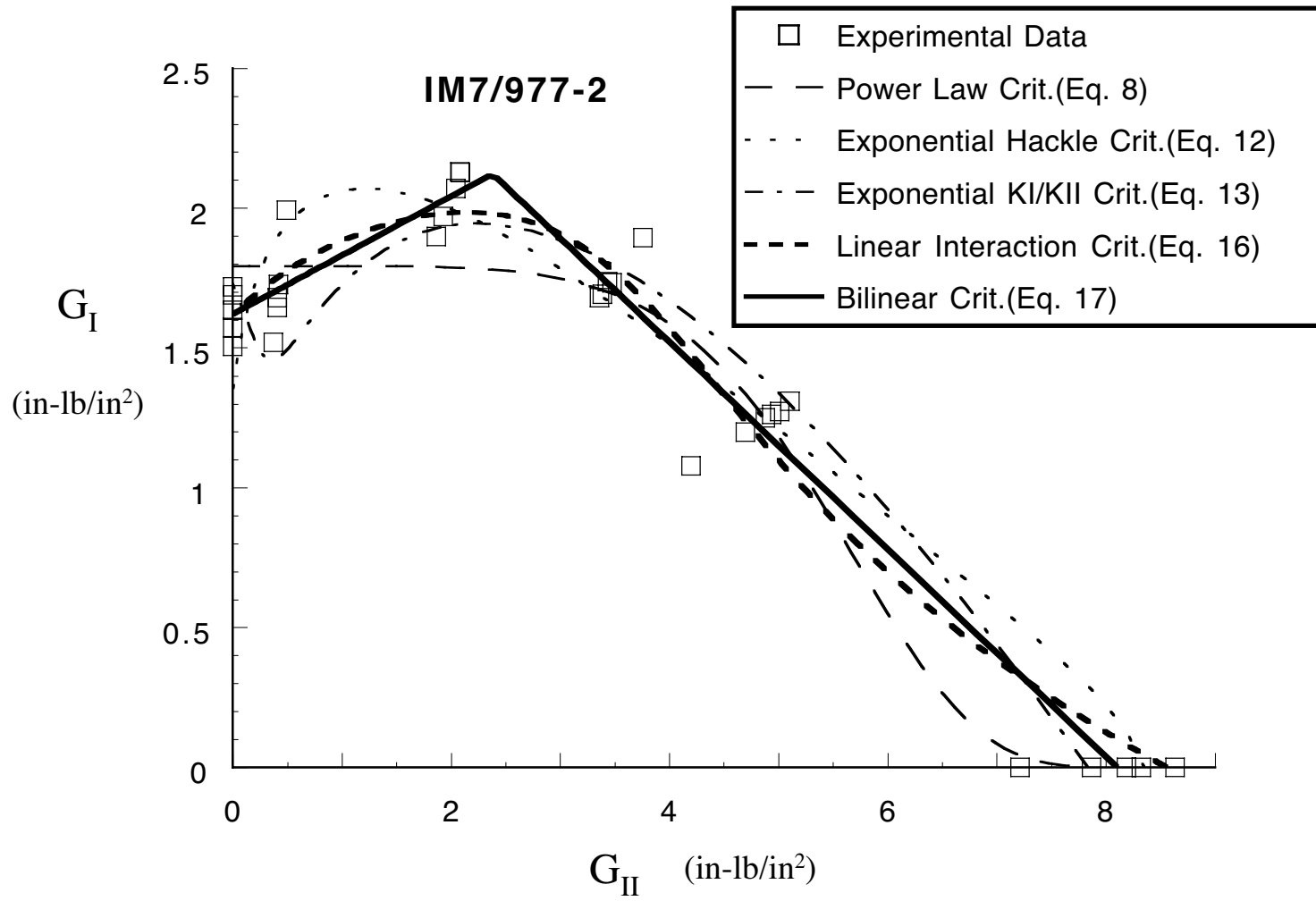


Figure 18. Mixed-mode toughness criterion curves for IM7/977-2.

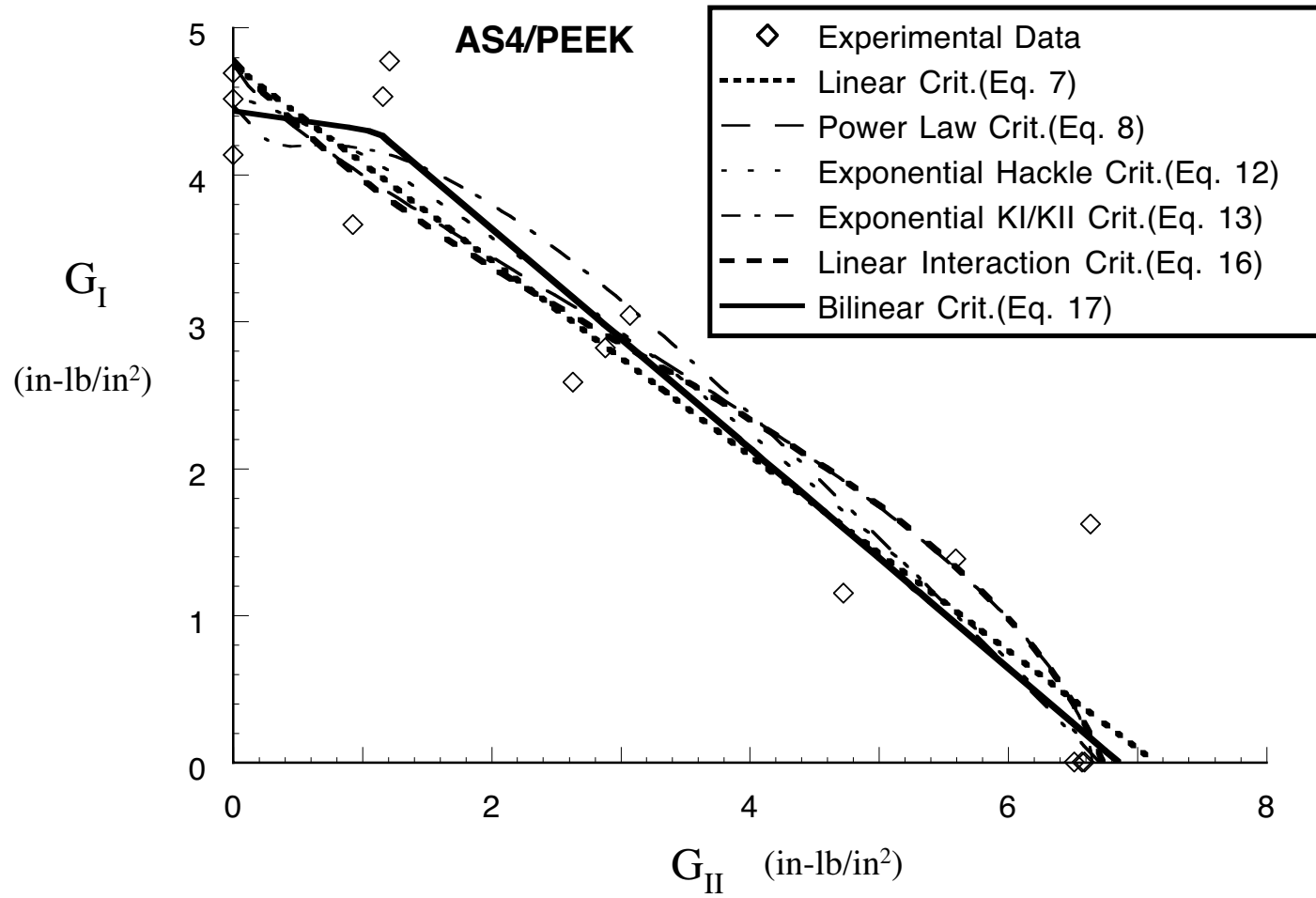


Figure 19. Mixed-mode toughness criterion curves for AS4/PEEK.

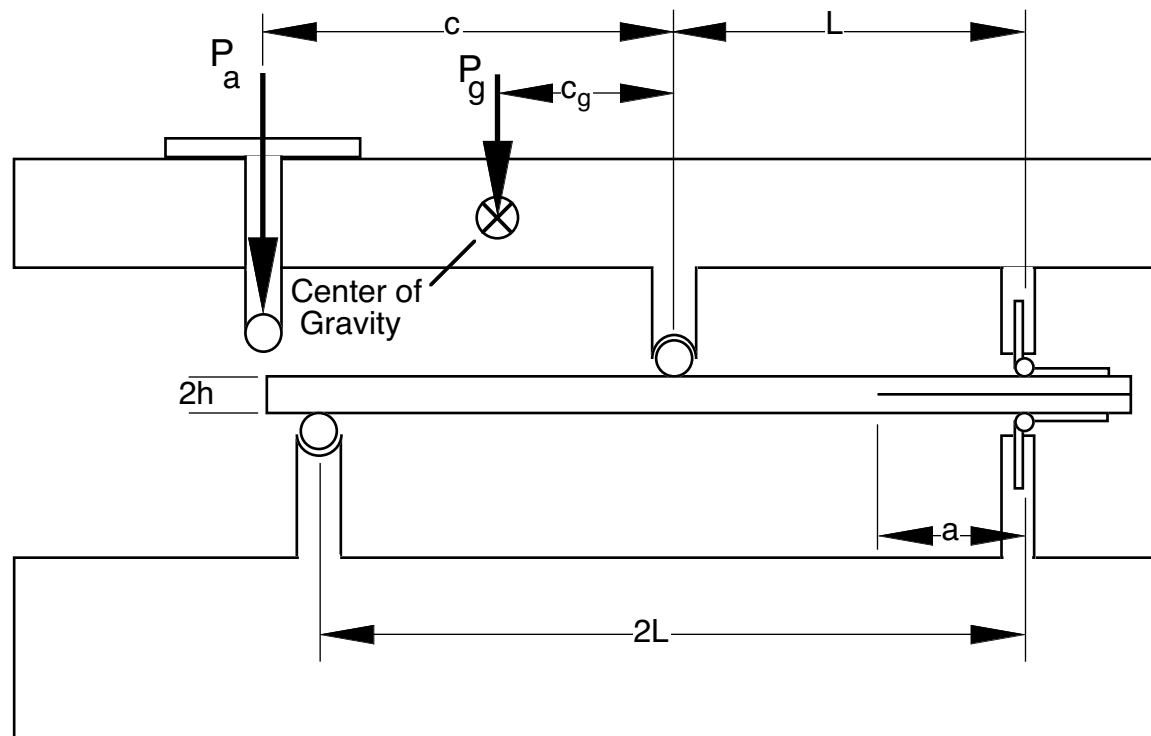


Figure A1. Lever weight applied to the improved mixed-mode bending test apparatus.

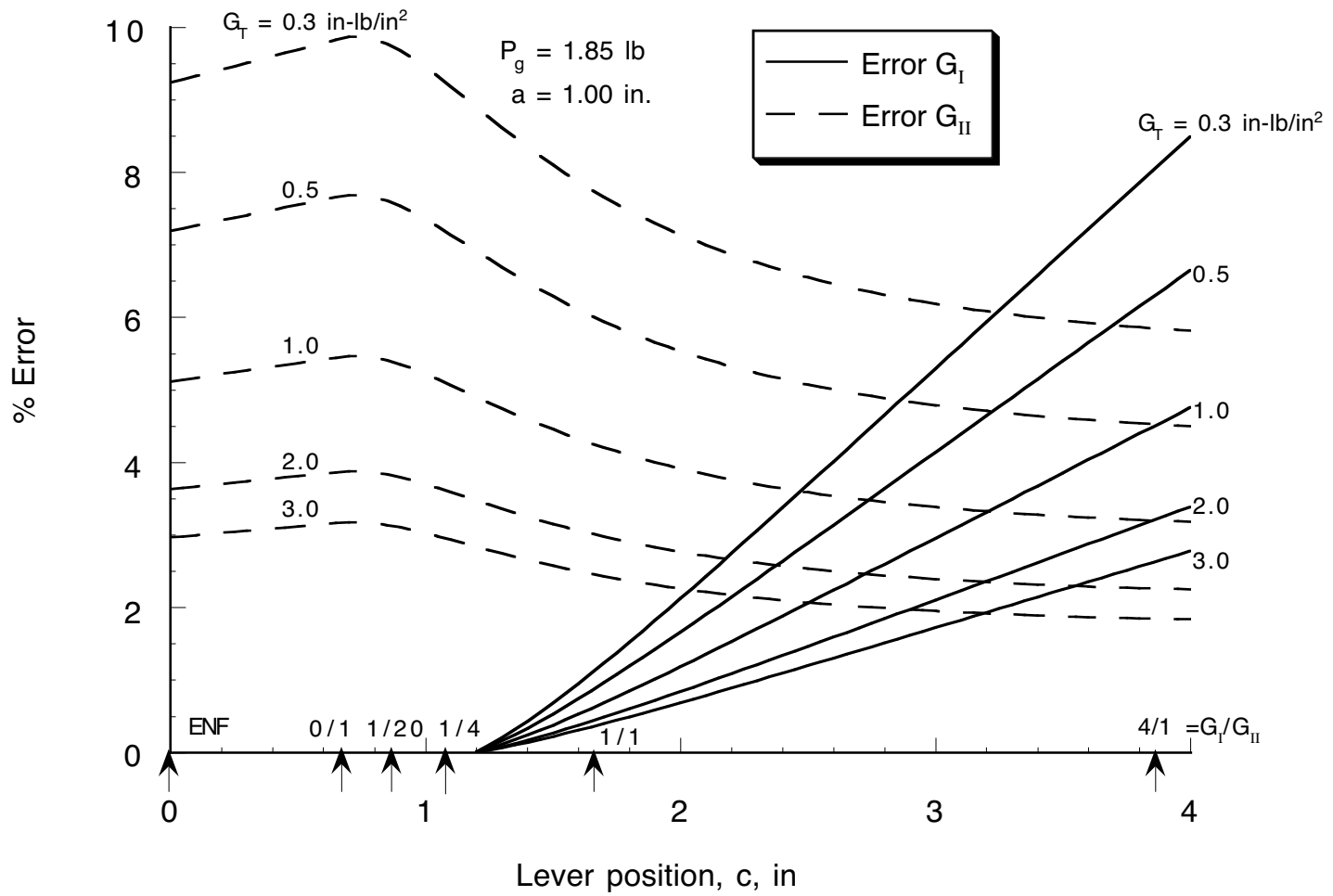


Figure A2. Effect of lever load position on G error due to lever weight